



Compendium solar spectrum formation

Robert J. Rutten^{1,2,3}

¹ Lingezicht Astrophysics, Deil, The Netherlands

² Institute of Theoretical Astrophysics, University in Oslo, Oslo, Norway

³ Rosseland Centre for Solar Physics, University in Oslo, Oslo, Norway

Abstract. The solar spectrum conveys most of our diagnostics to find out how our star works. They must be understood for utilization, but solar spectrum formation is complex because the interaction of matter and radiation within the solar atmosphere suffers non-local control in space, wavelength, and time. These complexities are summarized and illustrated with classic literature.

Contents

1	Introduction	1
2	On-line material	3
3	RT basics	4
	Intensity.	4
	Matter–radiation interactions.	4
	Bound-bound, bound-free, free-free interactions.	4
	Pair combinations.	4
	Equilibria.	4
	Bound-bound redistribution.	5
	Bound-free redistribution.	6
	Free-free redistribution.	6
	Thomson and Rayleigh scattering.	6
	Extinction and emissivity.	6
	Emission measure.	7
	Source function.	7
	Line source function.	7
	Transfer equation along the beam.	8
	Transfer equation in optical depth.	8
4	LTE: Holweger models	9
5	NLS: Auer & Mihalas modeling	10
6	NLS+NLW: Avrett models	10
7	NLS+NLW+NLT: Oslo simulations	12
8	NLS–NLW–NLT chromosphere spectrum	13
9	Conclusion	15

Table 1. Abbreviations, first RT ones, then my on-line RT material.

RT = radiative transfer ~ fermion-boson changes of I_ν
TE = thermodynamic equilibrium ~ detailed balance in all
LTE = local thermodynamic equilibrium ~ SB
NLTE = non-local thermodynamic equilibrium ~ SE
non-E = non-equilibrium ~ no SE
SB = Saha-Boltzmann populations ($\Rightarrow S_\nu$ equals $B_\nu(T)$)
SE = statistical equilibrium ~ all populations stable
CE = coronal equilibrium ~ SE + thin collisional creation
DEM = differential emission measure ~ CE density part j_ν
EM = emission measure $\equiv \int \text{DEM}(T) dT$
NLS = non-local in space ~ J_ν important
NLW = non-local in wavelength ~ other J_ν important
NLT = non-local in time ~ non-SE with memory
CS = coherent scattering ~ monofrequent, monochromatic
CRD = complete redistribution ~ sample extinction profile
PRD = partial redistribution ~ mix CS and CRD
ISSF = introduction to solar spectrum formation
IART = introduction to astrophysical radiative transfer
RTSA = radiative transfer in stellar atmospheres
SSI = introduction to solar spectrum formation
SSF = solar spectrum formation theory
SSX = solar spectrum formation examples
SSA = stellar spectra A (Cannon – Payne – Minnaert)
SSB = stellar spectra B (Avrett – Chandrasekhar – Unsöld)
SSC = stellar spectra C (Mihalas – Judge – Feautrier)

1. Introduction

The solar spectrum caused the dawn of astrophysics in the nineteenth century in the hands of Fraunhofer, Herschel, Kirchhoff and Bunsen, and others. Followed by stellar spectrum classification at Harvard by many ladies but foremost Cannon [SSF (pdf 2 ff)] – I invite you to now do practical SSA 1.1 (pdf 5) before reading further¹. In the twentieth century stellar spectrum interpretation evolved from basic concepts to understanding with Schwarzschild, Russell, Milne, Eddington, Minnaert, Chandrasekhar and others. Major breakthroughs were Payne’s demonstration with the Saha law that Cannon’s classification represents temperature ordering, the Pannekoek–Wildt–Chandrasekhar identification of H⁺ as major continuous opac-

¹ This [scissors-only exercise \(pdf 5\)](#) is illuminating. My website shows [photos](#) of many colleagues doing it, but young kids tend to do better than astrophysicists because they regard spectra without prejudice – just as Mrs. Cannon whose ordering into “early type – late type” suggests counting lines as wrinkles. *Spoiler: answer.*

ity provider, and Grotrian’s establishing the high temperature of the corona (recognizing its pearly eclipse visibility as Thomson scattering by fast electrons and identifying the optical emission lines as Edlén high-ionization transitions). Solar spectrum interpretation went from LTE (Unsöld) to NLTE with Menzel, Hummer, Thomas, Athay, Jefferies, Mihalas, Avrett and others. Then started (M)HD simulation modeling by Nordlund, Schüssler, Stein, Carlsson, Steiner and others with spectral synthesis codes by Carlsson, Uitenbroek, Heinzel, Leenaarts, Pereira and others, presently emphasizing the new frontier of non-E interpretation. ADS serves nearly all these works.

This text gives a brief overview dividing radiative transfer (RT) complexities between nonlocal in space (NLS), nonlocal in wavelength (NLW), nonlocal in time (NLT). Solar physicists generally appreciate NLS more than NLW and NLT.

arXiv:2103.02369v1 [astro-ph.SR] 3 Mar 2021

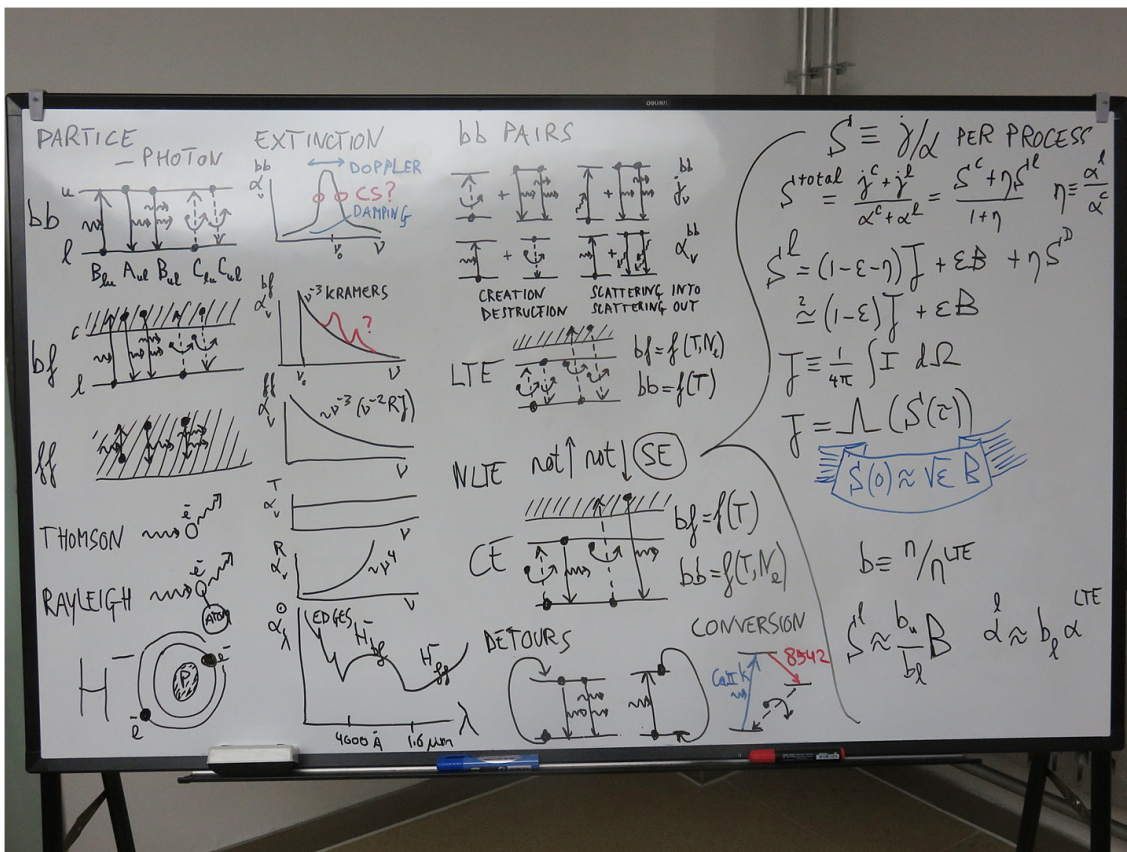


Fig. 1. Snapshot course summary, October 2018, Shandong University, Weihai. First column: particle–photon processes. Second column: corresponding extinction profiles. Third column: process pairs. Last column: key equations. Later I signed this painting.

BASIC QUANTITIES

Monochromatic emissivity

$$dE_\nu \equiv j_\nu dV dt d\nu d\Omega \quad dI_\nu(s) = j_\nu(s) ds$$

units j_ν : $\text{erg cm}^{-3} \text{s}^{-1} \text{Hz}^{-1} \text{ster}^{-1}$ I_ν : $\text{erg cm}^{-2} \text{s}^{-1} \text{Hz}^{-1} \text{ster}^{-1}$

Monochromatic extinction coefficient

$$dI_\nu \equiv -\sigma_\nu n I_\nu ds \quad dI_\nu \equiv -\alpha_\nu I_\nu ds \quad dI_\nu \equiv -\kappa_\nu \rho I_\nu ds$$

units: cm^2 per particle (physics) cm^2 per $\text{cm}^3 = \text{per cm}$ (RTSA) cm^2 per gram (astronomy)

Monochromatic source function

$$S_\nu \equiv j_\nu / \alpha_\nu = j_\nu / \kappa_\nu \rho \quad S_\nu^{\text{tot}} = \frac{\sum j_\nu}{\sum \alpha_\nu} \quad S_\nu^{\text{tot}} = \frac{j_\nu^c + j_\nu^l}{\alpha_\nu^c + \alpha_\nu^l} = \frac{S_\nu^c + \eta_\nu S_\nu^l}{1 + \eta_\nu} \quad \eta_\nu \equiv \alpha_\nu^l / \alpha_\nu^c$$

thick: (α_ν, S_ν) more independent than (α_ν, j_ν) stimulated emission negatively into α_ν, κ_ν

Transport equation with τ_ν as optical thickness along the beam

$$\frac{dI_\nu}{ds} = j_\nu - \alpha_\nu I_\nu \quad \frac{dI_\nu}{\alpha_\nu ds} = S_\nu - I_\nu \quad d\tau_\nu \equiv \alpha_\nu ds \quad \tau_\nu(D) = \int_0^D \alpha_\nu ds \quad \frac{dI_\nu}{d\tau_\nu} = S_\nu - I_\nu$$

Plane-parallel transport equation with τ_ν as radial optical depth and μ as viewing angle

$$d\tau_\nu \equiv -\alpha_\nu dz \quad \tau_\nu(z_0) = -\int_\infty^{z_0} \alpha_\nu dz \quad \mu \equiv \cos \theta \quad \mu \frac{dI_\nu}{d\tau_\nu} = I_\nu - S_\nu$$

start index

Fig. 2. Screenshot of [SSF (pdf 23)]. SSF offers 119 theory displays with a most negative evaluation [SSF (pdf 120)]. SSX offers 185 example displays. SSI offers only 16 introductory displays – you might start with these. Clicking the title of a display should return you to the previous shown display. The “start” button at the bottom should jump to the clickable contents overview, “index” to a clickable thumbnail index.

NLS means that radiation received from the location we are studying is influenced by local radiation there that came from elsewhere. It is daily familiar to us since our daytime outdoors is NLS illuminated. Whether sunshine or overcast, all photons we see were made in the Sun and made it into our eyes by scattering, mostly multiple. As NLS as it can get! Very much out of LTE since the radiation temperature is about 6000 K, higher than our local temperature².

NLW means that radiation received from the location we are studying is influenced by radiation at other wavelengths at that location. We do not suffer NLW because sunshine scattering around us is monochromatic (monofrequent): every detected photon still has the energy (frequency, color) with which it left the Sun. All solar Fraunhofer lines also reach our retinas unmo- lested (but disk-averaged and unnoticed³). We see the sky blue and the setting Sun red not because of underway color change but because Rayleigh scattering off molecules has higher probability at shorter wavelength. The green flash⁴ combines that with larger refraction in the blue.

NLT means that radiation received from the location we are studying is influenced by what happened there or thereabouts earlier. We suffer outdoors NLT because our sunshine is eight minutes retarded – but the same for all photons so we don't care.

Solar NLS defines outward decline of the line source function (what I call $\sqrt{\epsilon}$ scattering) that is well exemplified by the Na I D lines and most exemplified by Ly α , but it also brightens ultraviolet continua in and from the solar atmosphere. More below.

Solar NLW is exemplified by most atomic lines having opacity deficiencies up to an order of magnitude from sensing the scattering ultraviolet continua in ionization. It is less commonly appreciated, for example not in profile-fitting “inversion” codes nor in spectral irradiance modeling. More below.

Solar NLT is exemplified by solar H α which is a NLS $\sqrt{\epsilon}$ scattering line but it is also very NLW because Ly α defines its extinction (opacity) and a loop ionizing per scattering Balmer continuum from $n=2$ with cascade recombination back to $n=2$ including H α photon losses contributes to its source function. It is also very NLT because this loop is controlled by the n_2 population which lags badly in gas that was first heated and then cools, as happens continuously in the dynamic structures constituting the solar chromosphere and even in long-lived filaments/prominences appearing as chromospheric material high in the corona. Solar NLT can reach many orders of magnitude but is ignored in almost all modeling by invoking statistical equilibrium (SE). More below.

Below I first list on-line material used here and then summarize the theory⁵ in Sect. 3, followed by classic examples in order of complexity in Sects. 4–7. Finally in Sect. 8 the hardest nut to crack: the spectrum of the chromosphere.

² Only our eyesight is adapted to this radiation temperature, although its precise bandpass was probably defined in our aquatic past by the transparency of sea water to sunlight, as for giant squids (whose eyes have similar design and might suit nighttime astronomers better).

³ Even when you look at your beloved although (s)he gets so richly adorned.

⁴ My most beautiful was from the Neemach Mata temple in Udaipur.

⁵ Except polarization. Solar spectropolarimetry is a specialist field; del Toro Iniesta (2007) is a good introduction, Landi Degl'Innocenti & Landolfi (2004) the comprehensive bible.

2. On-line material

For brevity and to avoid repetition I much refer to teaching materials on my website⁶ using hyperlinks and therefore strongly recommend on-screen on-line pdf reading⁷. This compendium may then be studied at different levels:

- read only the main text of Sect. 3 and go through the SSF displays for a theory overview. The [SSX (pdf 72)] ff graphs of spectrum formation in the ALC7 star (Sect. 6) are suited exercise and self-examination material;
- also read the main text of Sects. 4–7 with some link inspection as overview of classic developments in solar spectrum modeling;
- also study the footnotes treating instructive cases of particular solar spectrum formation⁸ with linked literature;
- read everything and open every link and study all underlying material = full-fledged comprehensive course on solar spectrum formation with this text serving as convenient pointer and page opener.

My teaching material is listed and linked in Table 1. The first three files are course notes. ISSF and IART are at bachelors level, RTSA is at masters or graduate level. RTSA is the most recent (only 25 years old), is linked at ADS and is therefore most frequently used. However, at Oslo and elsewhere IART is preferred as easier and broader course material. ISSF was an introduction to Sac Peak summer students. IART follows Rybicki & Lightman (1986) with most emphasis on explaining their first chapter summarizing basic RT up to NLS treatment. RTSA was intended as an easier-to-read rehash of Mihalas (1970) with emphasis on solar NLS $\sqrt{\epsilon}$ scattering and adding NLW in particular for solar bound-free continua. None of these courses includes NLT nor the detour term in the line source function (Eqs. 2 and 3 below) which lacks even in Hubeny & Mihalas (2014). I included them in more recent summary tutorials in Rutten (2017a) and Rutten (2019).

The next three files in Table 1 are sets of projection displays that I use in teaching since the passing of the viewgraph era⁹. SSI is bachelors level, SSF and SSX are masters–graduate level. These also contain newer NLT aspects. I use(d) these displays during the workshop. Many have blue clickers that open figures and movies elsewhere in my laptop that won't work for you.

The final three files in Table 1 are practicals. They date back to the 1990s and therefore use IDL but are easily coded in Python. I highly recommend SSA and SSB, designed to accompany IART, for fresh RT students to gain hands-on insights. The third is a practical for RTSA developed by former graduate students that still awaits conversion into proper SSC format.

⁶ Search for “Rob Rutten webstek”. Presently these reside under https://webspacescience.uu.nl/~rutte101/Course_notes.html and <https://webspacescience.uu.nl/~rutte101/rweb/rjr-edu/exercises>.

⁷ An off-line or slow-connection alternative is to download these files first, open them in parallel, and use the pdf page number specified in each link (but no good for other weblinks and ADS page openers). This may especially suit SSX which is the largest.

⁸ Naturally a personal selection of cases that I have been involved in because these I know best and they came first to mind in this hurried quickie writeup – including 16: Ba II 4554 Å, 16: Mn I lines as activity monitor, 26: Thomas’ “photoelectric control”, 31: classical abundance determination, 32: Mg I 12 micron emission lines, 35: Milne-Eddington approximation; 38: standard-model line haze modeling, 41: quiet-Sun H α formation, 43: coronal heating by acoustic waves and gravity waves, 52: transition region, 56: ALMA chromosphere, 58: Ellerman bombs.

⁹ I still supply 90 viewgraph pages with all equations of RTSA in its equation compendium. The first few are empty.

Here I refer to these nine files for formalisms and equations that otherwise would swamp this summary and instead discuss issues and add footnoted asides – as I would do in oral 3D bodily-on-the-spot teaching while projecting and discussing the displays and publication pages that you should open and scrutinize yourself here. Square-bracketed hyperlinks¹⁰ to these files should open the particular page in your browser when you click on them¹¹. Similarly, many citations have [page links](#) to the pdf on ADS that should open the cited page.

3. RT basics

Figures 1 and 2 show overviews. Table 1 specifies acronyms I bombard you with¹².

Intensity. The basic RT quantity is specific intensity I_ν , describing energy in a beam of photons at a given location at a given time at a given frequency in a given direction, measured per units of area, time, frequency bandwidth and beam spreading [ISSF Sect. 3.1 (pdf 9)] [IART Sect. 2.1 (pdf 22)] [RTSA Eq. 2.1 (pdf 29)]. It is an ingenious macroscopic way to express that photons are bosons that do not decay and can travel through the whole universe without change and convey the whole universe to us for inspection.

Common sense suggests that the Sun is brighter than a distant star, but that is irradiance which is flux: if the distant star is solar-type it shows the same intensity, also when your time-travel starship parks you just above its surface. If your giant ground-based telescope resolves it the stellar intensity in the focus is the same as the solar intensity in the focus of DKIST¹³. Check [SSF (pdf 25)].

Matter–radiation interactions. Photons live forever¹⁴ after their creation unless they meet fermions and interact. Also their cre-

¹⁰ Colored blue to also suit dichromats. The suggestion is to click on blue items until you get blue in the face – meaning lack of sub-skin scattering by blood sunk in brain drain (‘tis all scattering here).

¹¹ With all pdf viewers I use, but some may instead shunt you to the first page. I add the pdf page number to these links for then going to the cited page. Acrobat may require undoing security settings disabling the opening of web pages.

¹² It would be good to hover your cursor over an acronym to pop up its meaning, best Wikipedia-style clickable for more. I have tried latex command pdftooltip in pdfcomment.sty for such popups but they worked too different between pdf viewers or not at all.

¹³ Solar telescopes are intensity telescopes and therefore photon-starved, worse when larger (nighttime colleagues won’t believe this). Reason: for pixels that resolve the diffraction limit (as they should) the flux of photons per pixel does not vary with aperture size, but smaller pixels sample smaller solar surface area (that’s the game) for which the solar change time (say crossing at solar sound speed) is faster. DKIST therefore needs four times faster data-taking cadences than the SST unless used as light bucket. This leaves four times less time for multi-frame collection for the required speckle or MOMFBD restoration. The latter technique needs fewer frames which is an important boon. At the DOT we used two-channel speckle reconstruction following Keller & von der Lühe (1992) to reduce speckle burst sizes in scanning through H α by adding wide-band imaging as is also done for SST MOMFBD (van Noort et al. 2005). It is easier to sample brightness = irradiance from a distant star with larger aperture yielding more photons as naively expected. On the other hand, fortunately our resolvable star kindly offers wavefront-encoding granulation everywhere on her surface so that we do not need a laser star for every isoplanatic patch.

¹⁴ Heeck (2013) concludes that they live at least 3 years – in their rest frame, meaning 10¹⁸ years for us.

ation is fermion business. For atoms, ions and molecules the photon-involving processes are bound-bound transitions producing spectral lines and bound-free and free-free transitions producing continua. In addition there are Thomson scattering of existing photons by free electrons and Rayleigh scattering of existing photons by bound electrons. Other photon-producing or photon-affecting processes may be ignored for the solar atmosphere unless you are a radio astronomer (cyclotron, synchrotron, plasma radiation) or high-energy astronomer (pair annihilation).

Photons being bosons means that they like to sit in the same place and therefore that any interaction producing or scattering a photon has a stimulated addition in which the new or scattered photon coherently accompanies similar passing radiation that enhances the interaction probability.

Bound-bound, bound-free, free-free interactions. The five bound-bound interactions are photo-excitation, spontaneous photo-deexcitation, induced photo-deexcitation, collisional excitation and collisional deexcitation [SSF (pdf 70)], [ISSF Sect. 5.1 (pdf 23)], [IART Chapt. 5 (pdf 60)], [RTSA Sect. 2.3.1 (pdf 39)]. The same five hold for bound-free ionization and recombination with appropriate nomenclature, and the same five hold for free-free interactions (but distinguishing collisional (three-body) up and down has no practical interest).

Pair combinations. Combining the above interactions in successive pairs is so important that I do not refer to or link to but copy Fig. 1 of Rutten (2019) here in Fig. 3. It came from [SSF (pdf 105)] and is an extension of [RTSA Fig. 3.3 (pdf 85)] with detours. Ca II and H α detour examples are shown in Fig. 2 (pdf 4) of Rutten (2019). Below I refer to these pairs by their alphabetic labels. Similar pair diagrams can be drawn for bound-free transitions.

Equilibria. See 2-level overview [SSF (pdf 69)] where the 2-level assumption means that any excitation is necessarily followed by de-excitation in the same transition, a didactic simplification that even applies sometimes, best to Ly α but also to ultraviolet bound-free continua.

TE = “*thermodynamic equilibrium*” describes a homogeneous isothermal fully-enclosed gas where nothing ever happens and where every type of excitation occurs just as frequently as its de-exciting counterpart (“detailed balance”): as many collisions down as up, as many radiative transitions down as up, with all rates defined by the temperature. Maybe this occurs approximately at the center of a black hole, but not within the Sun since non-enclosed implies net outward energy transport and the accompanying outward temperature decline everywhere.

SE = “*statistical equilibrium*” foregoes detailed balancing but requires overall balancing, meaning that the level populations do not vary with time however they are made. This assumption underlies all following equilibria except non-E.

LTE = “*local thermodynamic equilibrium*” assumes TE at the local temperature while permitting temperature and density gradients and small leaks, clearly a cheap cheat. Its definition is that Saha-Boltzmann (SB) partitioning applies to all populations, as for element Schadeenium in the recommended SSA 2 Cecilia Payne exercise (pdf 9). It is often thought that LTE is defined as equality of the source function S_ν to the Planck function B_ν but this is a corollary [RTSA Sect. 2.3.2 (pdf 43)]. LTE holds closely within the Sun and to some extent for many lines

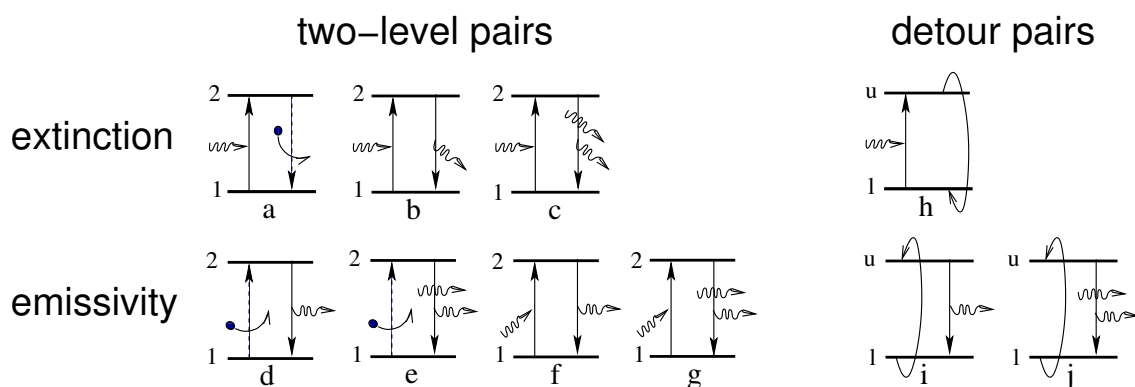


Fig. 3. Atomic transitions governing line formation arranged in photon-involving pairs. The intensity in the beam of interest travels from left to right. Detour paths (righthand cartoons) combine transitions involving other levels and may include analogous bound–free transitions. The upper row shows pair combinations contributing to line extinction: collisional photon destruction (**a**), scattering out of the beam (**b** and **c**), photon conversion out of the beam (**h**, into other-wavelength photons and/or kinetic energy). The lower row shows pairs contributing to line emissivity: collisional photon creation (**d** and **e**), scattering into the beam (**f** and **g**), detour photon production into the beam (**i** and **j**). Pairs **c** and **g** have equal probability by requiring one photon in the beam and one with arbitrary direction.

and continua in the low photosphere. The condition is that collisions both up and down heavily outweigh photons up and down in Fig. 3 and its bound-free counterparts: photon destruction **a** and photon creation **d** + **e** must dominate over spontaneous and stimulated scattering, also for all steps in the photon conversion sequences at right. Thus, the photons must behave as “honorary gas particles” (Castor), likewise boxed in to local circumstances; what we observe must be only a small leak. In SB partitioning the level population ratios sense only the temperature [RTSA Eq. 2.86 (pdf 49)] because the dominating up and down collisions both require one collider so that the density drops out. The ionization stage ratios sense temperature more complicatedly by mixing the Boltzmann factor with the Maxwell distribution for the caught electron into the Saha distribution [RTSA Eq. 2.88 (pdf 50)] and scale inversely with the electron density by the need to catch one.

NLTE = “non-local thermodynamic equilibrium” is a misnomer. Usually it means assuming SE with accounting for NLS, less often NLW, much less often NLT.

CE = “coronal equilibrium” assumes SE but absence of local irradiation so that only **d** and its bound-free counterpart remain. Every photon is locally created by a collision obeying the local kinetic temperature and escapes outward to space or drowns inward in the Sun or gets bound-free scattered in overlying gas (more below). In this case the level ratios sense both temperature and collider density since there is only the required bound-bound up collision, not the down one additionally required for LTE. The stage ratios sense only temperature because each ionization is collisional and each recombination is radiative requiring a single electron catch. A numerical complication is that dielectronic recombination must be included. The reason is that at coronal temperatures the mean Maxwellian energy gets far above the zero value desired at ionization threshold. Dielectronically the kinetic energy is cut down by using part for simultaneous valence-electron excitation. The reverse process is called auto-ionization. Classical Fig. 3 (pdf 20) of Jordan (1969)¹⁵ shows its importance for iron partitioning (the lower panel shows partitioning without it from House 1964). Because

¹⁵ Carole Jordan is the CE counterpart of SB Cecilia Payne, moving to Oxford from Culham rather than to Cambridge USA from Cambridge UK. My SSA exercises should become Annie Cannon – Cecilia Payne – Carole Jordan, likely using CHIANTI, and also add a Walter Grotrian [SSX (pdf 6)] exercise.

the ratio direct–dielectronic recombination depends only on temperature (Maxwell-peak shift) the dielectronic addition maintains the temperature-only sensitivity of CE stage partitioning. CE and SB are thin versus thick partitioning extremes. [SSX (pdf 174)] compares them for photospheric electron density; the SB peaks shift left by about -0.05 in $\log(T)$ per tenfold N_e reduction.

Non-E = “non equilibrium” means non-SE = NLT, admitting temporal variations in populations, i.e., having the SE population equations [RTSA Eq. 2.100 (pdf 52)] not equaling zero but a function of time. For hydrogen it is often called “non-equilibrium ionization” but this is a misnomer because the actual agent is NLT slow collisional settling of Ly α in cooling gas whereas H ionization occurs in an SE Balmer loop (more below).

Bound-bound redistribution. Eddington asked on page 2 (pdf 2) of Eddington (1929) the “crucial question” to what extent a resonance-scattered photon remembers the frequency it had in the preceding photo-excitation (pairs **b**, **c**, **f**, **g**). The one extreme is that it does precisely in “coherent” scattering (CS). In Eddington’s days this was thought to be the rule, but in his brilliant thesis Houtgast (1942) showed that most solar lines in the visible obey the other extreme, suffering complete redistribution (CRD) meaning complete loss of memory and representing a new sample of the line extinction profile rather than δ -function frequency conservation. CRD is indeed valid for most lines except the strongest (large extinction) because their photons escape high in the atmosphere where collisions governing collisional redistribution (“damping”) are rare. These must be described by partial redistribution (PRD) which combines Doppler redistribution in the core (CS in the frame of the atom but an redistributing average over the observed individually-Doppler-shifted photon ensemble) with coherency in the inner wings and collisional redistribution in deeply-formed hence collision-rich outer wings [SSF (pdf 89)]. The best-known examples are Ly α , Mg II h & k, Ca II H & K [SSF (pdf 92)], [SSF (pdf 93)]. My personal example is Ba II 4554 Å¹⁶. I must concede that this issue remains “not

¹⁶ Ba II 4554 Å showed PRD signature near the limb in my eclipse observation in Fig. 9 (pdf 17) of Rutten (1978). It was confirmed in Figs. 1–3 (pdf 4) of Rutten & Milkey (1979) and Fig. 6 (pdf 5) and Fig. 11 (pdf 7) of Uitenbroek & Bruls (1992). The line is a valuable spectropolarimetry diagnostic (Belluzzi et al. 2007) and also a good

yet” in [RTSA Sect. 3.4.3 (pdf 92)]. The clearest explanation so far is in Chapter 5 (pdf 110) of Jefferies (1968)¹⁷, summarized in [SSF (pdf 91)]. The introduction to Sukhorukov & Leenaarts (2017) is a good literature overview. Recent developments are listed in [SSX (pdf 164)]. Next to frequency redistribution there is also angle redistribution to worry about for moving gas due to its Doppler anisotropy – what gas in the solar atmosphere doesn’t move? See Leenaarts et al. (2012b).

Bound-free redistribution. Bound-free transitions are very similar to bound-bound transitions and may be described by the same rate equations [RTSA Sect. 3.2.3 (pdf 68)]. However, recombination requires catching an electron as a fresh sample of the kinetic energy distribution without knowledge of the electron kicked out in preceding ionization. There is knowledge = memory of ionization to the threshold but not of the excess above it imparted as kinetic energy. Hence there is always CRD over the ionization edge and that is also much wider in spectral extent than a spectral line.

A particular case is bound-free scattering of EUV line photons imaged in narrow bands as by EIT, TRACE, AIA. They may be extincted in bound-free photo-ionization of HI, He I or He II, most likely followed by spontaneous photo-recombination because the colliding-particle and suited-photon densities are too low for other bound-free equivalents than scattering pair **b**. Through CRD such a bound-free scattered photon not only gets a random redirection but also a new wavelength, most likely near the ionization threshold (probability for HI given by Kramers ν^{-3} decay [RTSA Eq. 2.74 (pdf 45)]), hence far from the line. Bound-free scattering so redirects radiation out of the line of sight and also out of the passband; it may locally darken the narrow-band image (often misnamed “absorption”). When you see the same black features on bright backgrounds (outside no-

Doppler diagnostic of the upper photosphere (Shchukina et al. 2009, Kostik et al. 2009) because it combines large atomic mass, hence small thermal broadening, with considerable core broadening by isotope splitting and hyperfine structure making it suited for filter instruments (Sütterlin et al. 2001). Other lines with large hyperfine broadening are the Mn I ones recommended by Elste to Livingston as candidates for long-term spectral irradiance monitoring because they are insensitive to infamous microturbulence (footnote 31). Livingston found larger cycle-dependent variation in Mn I 5394.7 Å than for other atomic lines (Fig. 16 (pdf 9) of Livingston et al. 2007). This enhanced sensitivity was attributed by Doyle et al. (2001) to pumping of Mn I 5394.7 Å by Mg II k but erroneously assuming CRD for Mg II k in the spectral synthesis of their demonstration. Vitas et al. (2009) showed that the actual reason is that hyperfine-broadened lines indeed lack the “microturbulent” thermal and granular Doppler smearing through which all narrower photospheric lines lose such sensitivity (MURaM demonstration in their Fig. 6 (pdf 8) and Fig. 7 (pdf 9)). I reviewed this issue in Rutten (2011, not on ADS but posted here) where Fig. 1 (pdf 2) summarizes Livingston’s results and Fig. 2 (pdf 3) shows that in plage the Mn I blend (at -0.7 Å from Mg II k center) is not pumped at all because the blend is at the wavelength where the PRD source function departs most from the CRD one and sits in the dip outside the Mg II peak even in strong plage. The apparent Mn I over Fe I brightening of plage in Fig. 1 (pdf 2) in scans from Malanushenko et al. (2004) results from mean-field brightness normalization. The surrounding granulation is actually darker in the Mn I line than in the turbulence-sensitive Fe I line while these lines show the same actual plage brightness because the fluxtube “holes” schematized in Fig. 4 (pdf 5) reach as deep because both Fe I and Mn I ionize away.

¹⁷ Scanned by Andrii Sukhorukov and put on ADS by me with author consent.

emissivity coronal holes) in multiple EUV wavelengths this out-of-the-passband scattering is the most probable mechanism¹⁸.

Free-free redistribution. Every collider is a fresh sample of the kinetic energy distribution giving redistribution over the probability ν^{-3} decay [RTSA Eq. 2.76 (pdf 46)], a continuum without threshold. In addition there is no memory of a preceding transition so that pair combinations as in Fig. 3 make no sense. If the kinetic energy distribution is the Maxwell distribution defined by temperature then that fully defines both emissivity (Brehmstrahlung) and extinction so that their ratio (source function) is the Planck function. Thus, free-free transitions always have $S_\nu = B_\nu$ because they are intrinsically collisional.

A particular case is ALMA for which at longer wavelengths the main agent is hydrogen free-free (electrons meeting protons) [SSX (pdf 32)]. ALMA is therefore often appreciated as a thermometer, but it is as often not appreciated that the extinction is likely NLT controlled and may be orders of magnitude above the local LTE value, just as for H α . ALMA is a thermometer but without easy knowledge where you stick it (more below).

Thomson and Rayleigh scattering. In terms of Fig. 3 these scatterings are described by pairs **b**, **c** and **f**, **g**, none of the others. In the Thomson limit (short of Compton) they still suffer Doppler redistribution. Pairs **c** and **g** cancel in occurrence probability, averaged for Doppler redistribution.

A particular case is Thomson scattering by free electrons making the white-light corona so beautifully visible [SSX (pdf 5)] during eclipses and with coronagraphs. Since this is monochromatic scattering the absence of photospheric Fraunhofer lines, unlike the spectrum scattered by your nose, was puzzling until Grotrian (1931) noticed that Ca II H & K are shallowly present and proposed here (pdf 22) that their 100 Å smearing corresponds to 7500 km s⁻¹ Doppler redistribution – but his attribution to thermal motion at million K temperature came later (I suspect he didn’t dare yet at the time). For smooth-disk illumination the scattered brightness is locally proportional to N_e , but as pointed out by Minnaert (1930) limb darkening (and perhaps spots) must be accounted for in the local scattering source function $S_\nu = J_\nu$, and also the integration along the entire line of sight with problematic confusion between different structures (evident in the marvelous Druckmüller images).

Extinction and emissivity. The extinction coefficient¹⁹ and the emissivity²⁰ are the macroscopic ways of quantifying the above processes locally along a given beam with given intensity (Fig. 2). See [SSF (pdf 23)] with more explanation in [ISSF

¹⁸ Cartoon explanation in Fig. 10 (pdf 12) of Rutten (1999) to answer a TRACE question by Karel Schrijver.

¹⁹ Naming: in many texts this is called “absorption coefficient”. I follow Kees Zwaan (whom I succeeded in teaching IART and RTSA) in using “extinction” because the photon is taken out of the particular beam (direction and frequency) but may still exist in another direction (scattering pairs **b** and **c**) or at another frequency (conversion pair **h**). Absorption is then reserved for pair **a** only, which has sometimes been called “true absorption”.

²⁰ Naming: Zwaan, Jefferies, Mihalas and others called this “emission coefficient”. I followed them in IART and also while writing RTSA in 1995, but at an Oslo school that summer Phil Judge used “emissivity” and I realized that that is a better name because it is not a coefficient, not a fraction of something but new radiation.

Sect. 3.2 (pdf 9)], [IART Chapter 3 (pdf 34)], [RTSA Sect. 2.1.2 (pdf 32)].

A particular point is that photons contributed by stimulated emission are not counted positively as contribution to emissivity but negatively as contribution to extinction. I suspect that this was first done by Einstein himself. It facilitates the description because extinction ($\mathbf{a} + \mathbf{b} + \mathbf{c} + \mathbf{h}$) and stimulated emission ($\mathbf{e} + \mathbf{g} + \mathbf{j}$) both need beam photons and therefore similar quantification (Einstein B values [SSF (pdf 70)]). Moreover, with this subtraction the cancelation of pairs \mathbf{c} and \mathbf{g} is effectuated. If this isn't done the actual extinction would be overestimated and optical depth scales would suggest larger opaqueness and higher escape than actually the case²¹.

Emission measure. Colleagues studying the coronal EUV spectrum usually do not worry about photons after their creation²². Optically thin travel to the telescope, no extinction, only emissivity counts in their production per pair \mathbf{d} . This must be evaluated for all lines within the passband²³ at every location along the line of sight and integrated with confusion an issue. Locally the emissivity scales with the product $n_l N_e$ of lower-level population density and electron density, the latter representing the required collider for excitation per \mathbf{d} which is most likely an electron. Regard a resonance line from an ion ground state. Its population enters as $(n_l/N_E) A_E N_H$ with element E abundance $A_E = N_E/N_H$, hence local emissivity $\propto g f A_E G_{ij}(T) N_e N_H$ where G_{ij} is a conglomerate function of temperature describing the element partitioning defining n_l/N_E for this line ij and needing all sophistication of **CHIANTI** for evaluation within the CE assumption. If the line is from an excited state function G_{ij} depends also on electron density. Integration over the volume of an unresolved emitting structure (say a loop) yields emission $\propto g f A_E \int G_{ij}(T) N_e N_H dV$ where N_H is often replaced by N_e taking $N_H = N_p \approx N_e (1 - 2B)$ with B the helium/hydrogen abundance ratio (Sect. 5 (pdf 20) of Pottasch 1964). The density dependencies $N_e N_H$ may be removed using the differential emission measure $DEM(T) \equiv N_e N_H (ds/dT)$ in $\text{cm}^{-5} \text{K}^{-1}$, a combined local gradient measure that defines the emission measure integrated over s along the line of sight as $EM \equiv \int N_e N_H ds = \int DEM(T) dT$ in cm^{-5} (Sect. 7 (pdf 113) of Del Zanna & Mason 2018). With this density removal the emission in the line from a feature becomes $\propto f A_E \int DEM(T) g G_{ij}(T) dT$ where the Gaunt factor g is under the integral because it depends on temperature (Eq. 2 (pdf 3) of Withbroe 1978).

Source function. I wonder who gave this key non-thin quantity its well-suited name in describing weighted local addition of new photons to a given beam by dividing emissivity and extinction (Fig. 2). It seems like dividing cows and horses since their dimensions are $[\text{erg cm}^{-3} \text{s}^{-1} \text{Hz}^{-1} \text{sr}^{-1}]$ versus just $[\text{cm}^{-1}]$, but

²¹ More in a [Dick Thomas memorial](#).

²² Solar physicists used to be either thin or thick. Thin ones excelled in atomic physics, thick ones in 2-level scattering and later in MHD. They now grow together. The Sun doesn't care and magnanimously sends photons to both types adhering to her "Principle of Solar Communicativity" (pdf 9) formulated at the only solar IAU symposium ever in the USSR (Rutten 1990).

²³ For filter instruments as AIA usually a complex multi-temperature combination. Spectrometers as Hinode/EIS select a single line but do not inform precisely where from – slitjaw imaging as by IRIS is highly desirable – or miss the more interesting happening just next to the slit. It is a pity that Fabry-Pérot imaging spectroscopy is not feasible at short wavelengths; SST/CHROMIS is the shortest (Scharmer et al. 2019).

the resulting dimension is that of intensity [SSF (pdf 23)] which 'tis all about.

The source function is a key quantity for optically thick colleagues (those studying the photosphere and chromosphere) because it separates local physics and surround physics, or atomic perspective and environmental quality. Take a strong spectral line, meaning large extinction coefficient. It produces a large narrow upward spike in extinction versus wavelength. This is local physics: the required particles must be present in sufficient number set by elemental abundance, partitioning over ionization stages and atomic levels within stages that is primarily set by temperature and density (closer to SB than to CE), and transition probability. In the emissivity there is a similar spike given by lookalike particles in the upper level. In the ratio, however, this spike may vanish completely – as for LTE with the featureless Planck function as ratio. Then the ratio is completely set by the temperature, an environmental rather than an atomic physics quantity. When LTE is not valid the local environment also senses nonlocalness, surely in space (NLS), likely also in wavelength (NLW), possibly also in time (NLT). Thus, optically thick colleagues evaluate local atomic properties to define the extinction which defines where their signal comes from, then evaluate the source function to see what environmental effects may make it depart from the local temperature. This split is often described as "accounting for NLTE".

However, such split interpretation gets mixed when environmental effects also affect the extinction. This happens when that is controlled by other transitions sensitive to source function nonlocalness. The extinction of visible atomic lines defined by scattering bound-free ultraviolet continua is one example, the dominance of $\text{Ly}\alpha$ in controlling $\text{H}\alpha$ extinction and ALMA HI free-free extinction is another. In such cases, opacity NLTE gets more important than source function NLTE. Colleagues that see NLTE only as a source function issue may miss the crux of their problem.

Also, the source function is a composite because it is a process property. Multiple processes operating at a given wavelength each have their own source function and combine weighted (Fig. 2) [SSF (pdf 23)]. In the solar photosphere optical lines often combine a scattering line source function with a near-LTE continuous source function because the latter is dominated by H^- bound-free interactions. These are not necessarily LTE as is the case for free-free interactions. In the ultraviolet bound-free continua do get far from LTE but in the optical and infrared ambient thermal kinetic energy is similar to or exceeds transition energy and at sufficiently deep formation²⁴ collisions reign, making LTE a good approximation. The Na I D lines reach deepest in the optical spectrum (Fig. 10 (pdf 18) of Rutten 2019) because they are exemplary $\sqrt{\epsilon}$ scatterers [SSX (pdf 85)]. In hotter stars where hydrogen is ionized the reverse occurs: weak LTE lines appear in emission on the dark Thomson-scattering continuum (Fig. 1 (pdf 215) of Rybicki & Hummer 1992). A weak solar NLW continuum-scattering emission line superposed on two strong $\sqrt{\epsilon}$ scattering absorption lines (Ca II H and H ϵ) is Fe II 3969.4 Å which responds deeper than its background (Fig. 8 (pdf 9) of Cram et al. 1980).

Line source function. Most classic treatments of NLTE scattering in the line source function assume a gas of 2-level atoms

²⁴ In the optical and near infrared solar continuous extinction is smallest so that we see deepest there (SSI pp. 5-7 (pdf 5 ff), [RTSA Fig. 8.6 (pdf 199)], Figure 6 (pdf 13) of Rutten (2019)). A true solar physicist (pdf 9) observing the Earth also sees deepest in the optical.

to keep the description monochromatic (CS) or limited to a single line (CRD). I did the same in RTSA, with a long derivation inventing “sharp-line atoms” enabling use of the Einstein coefficients in [RTSA Sect. 3.4 (pdf 84)], an elegant derivation by Zwaan of the $\sqrt{\varepsilon}$ law in [RTSA Sect. 4.3.1 (pdf 112)], and the classic numerical CRD results for this law in an isothermal atmosphere of Avrett (1965) in [RTSA Sect. 4.3.5 (pdf 124)]. An equation summary is shown in [SSF (pdf 79)] and as [RTSA concluding rap (pdf 275)].

Two-level scattering source function evaluation became a key part of numerical spectrum synthesis with many codes following the key concepts of opposite-direction averaging of Feautrier (1964) [RTSA Sect. 5.2 (pdf 137)] and of operator splitting of Cannon (1973), leading to approximate lambda iteration (ALI) and similar methods [RTSA Sect. 5.3.2 (pdf 145)]. Some of these codes are detailed below in Sects. 4–6²⁵.

The extension with detours is still lacking in my courses, so I add that here. The best description so far is in Sect. 8.1 (pdf 199) of Jefferies (1968) (remove the minus in the equation below Eq. 8.8). Split the line extinction coefficient into the destruction (a for absorption), scattering (s), and detour (d) contributions of Fig. 3:

$$\alpha'_\nu \equiv \alpha_\nu^a + \alpha_\nu^s + \alpha_\nu^d \quad \varepsilon_\nu \equiv \alpha_\nu^a / \alpha'_\nu \quad \eta_\nu \equiv \alpha_\nu^d / \alpha'_\nu \quad (1)$$

where ε is the collisional destruction probability of an extincted photon and η is its detour conversion probability. With these, the general line source function becomes

$$S_\nu^l = (1 - \varepsilon_\nu - \eta_\nu) J_\nu + \varepsilon_\nu B_\nu(T) + \eta_\nu S_\nu^d \quad (2)$$

for CS and

$$S_{\nu_0}^l = (1 - \varepsilon_{\nu_0} - \eta_{\nu_0}) \overline{J_{\nu_0}} + \varepsilon_{\nu_0} B_{\nu_0}(T) + \eta_{\nu_0} S_{\nu_0}^d \quad (3)$$

for CRD with $\overline{J_{\nu_0}} \equiv (1/4\pi) \iint I_\nu \varphi(\nu - \nu_0) d\nu d\Omega$ the “mean mean” intensity averaged over all directions and the line profile, with ν_0 the line-center frequency and also used as line identifier. The first term in Eqs. 2 and 3 represents the reservoir of photons that contribute new photons to the beam by direct scattering (**f** and **g**), the second describes collisional beam-photon creation (**d** and **e**), the third the contribution of new beam photons via detours (**i** and **j**) which themselves may contain collisional, scattering and also such bound-free steps.

Equations 2 and 3 show that LTE $S = B$ equality holds when $\varepsilon = 1, \eta = 0$ and/or $J = S^d = B$, both true below the standard $h = 0$ surface at $\tau_{5000}^c = 1$. Above it ε becomes small from lower electron density while η is usually smaller²⁶. All bound-bound lines and bound-free continua formed above a few hundred km height are heavily scattering with $S \approx J$ (but free-free continua always have $S = B$ because each interaction is collisional).

²⁵ An online tool for hands-on experimentation with various methods is at <http://rttools.irap.omp.eu> and described by Lambert et al. (2016). It produces plots as [RTSA Fig. 5.2 (pdf 147)] on your screen.

²⁶ $H\alpha$ has a sizable ηS^d contribution from bound-free detours as the loop shown in Fig. 2 (pdf 4) of Rutten (2019). It was famously called “photoelectric control” by Thomas (1957) with a schematic source function diagram in Fig. 3 (pdf 5) of Jefferies & Thomas (1959) that was reprinted in Fig. 12-9 of Mihalas (1970) and Fig. 11-11 of Mihalas (1978). It is qualitatively similar to the $H\alpha$ source function in [SSX (pdf 91)] with S'_ν leveling out in the photosphere to become much higher than B_ν in the temperature minimum – but the “photoelectric control” designation was wrong because even this complex line is mostly scattering as shown in Fig. 12 (pdf 9) of Rutten & Uitenbroek (2012) who found that the upper-photosphere excess is due to backscattering from the chromosphere. Towards the limb such backscattering can also be seen as $H\alpha$ brightening under filaments (Kostik & Orlova 1975).

Transfer equation along the beam. See [ISSF Sect. 3.3 (pdf 10)] for a gentle introduction. Here τ_ν is optical thickness measured in the beam direction. [ISSF Figure 5 (pdf 14)] treats a spectral line from a homogeneous isothermal cloud with LTE processes, say a galactic HI cloud showing the 21-cm line to a radio astronomer. Of my cartoon diagrams this one is most often shown, nowadays as Python animation. Appreciate how the line grows or sinks with increasing cloud opacity until it hits the optically thick limit. Thick isothermal LTE clouds show no lines (as black holes have no hair).

Transfer equation in optical depth. For very optically thick objects there is no interest in what impinges the other side if nothing comes through. We then flip τ to measure optical depth instead, either against the line of sight ($\tau_{\nu\mu}$) or more often against height radially into the Sun. The standard recipe is then to apply the Eddington-Barbier²⁷ approximation as indicator of “height of formation” [ISSF Eq. 35 (pdf 13)], [IART 321 (pdf 45)], [RTSA Eq. 2.44 (pdf 38)], [RTSA Eq. 4.32 (pdf 106)], [SSF (pdf 29)] and [SSF (pdf 51)]. The “four-panel” diagrams in [SSF (pdf 31)]–[SSF (pdf 38)] are a graphical course on Eddington-Barbier spectrum formation with increasing complexity. You should blink the absorption–emission pairs by full-page flipping.

Be aware that the Eddington-Barbier approximation may fail miserably: do the exam on [SSF (pdf 40)]. If you assign $h \approx 150$ km to the blend by reading off where its center intensity equals the source function (which works very well for Na I D₂) you are a million times wrong...²⁸

Be also aware that solar-atmosphere structures may be optically thick without being effectively thick so that radiation scatters through. Filaments or fibrils may appear intransparent in $H\alpha$ while illumination from behind is still important. This is even the case for $H\alpha$ in the “chromosphere” plateau of 1D standard models, as in [SSX (pdf 91)] which not only shows $S \approx J > B$ across the model temperature minimum from backscattering treated in footnote 26 but also has photospheric photons scattering through the model chromosphere. This caveat was beautifully demonstrated in Fig. 7 (pdf 7) of Leenaarts et al. (2012a) by comparing 1D $H\alpha$ synthesis for a Bifrost simulation with MULTI²⁹ of Carlsson (1986) and 3D $H\alpha$ synthesis with MULTI3D³⁰ of Leenaarts & Carlsson (2009). In the columnar 1D line synthesis the deep-photosphere granulation is better visible than lower-contrast chromospheric fibrils but in 3D synthesis the granular contrast is smoothed away by sideways scattering.

The most important equation of classical 1D 2-level scattering is the Schwarzschild equation defining the Λ operator [RTSA Eq. 4.14 (pdf 98)]; a synopsis is given in (pdf 9–10) of Rutten (2019). Its cutoff at the surface produces outward $J_\nu < S_\nu$ divergence for small inward increase of $S_\nu(\tau_\nu)$ but outward $J_\nu > S_\nu$ divergence for steep increase [RTSA Fig. 4.2 (pdf 100)], [RTSA Fig. 4.4 (pdf 103)], [RTSA Fig. 4.9 (pdf 121)]. Be aware that

²⁷ Unjustly named (Paletou 2018) – as more often with Eddington.

²⁸ The same graph is also the subject of [RTSA Problem 7 (pdf 250)].

²⁹ Spectrum synthesis: MULTI initially used linearization following Scharmer & Carlsson (1985) with the brilliant [RTSA Scharmer operator (pdf 148)] (yes, the same as the brilliant SST builder) to obtain J_ν rather than J_ν from S_ν with a local Eddington-Barbier approximation. It was later extended with the diagonal [RTSA OAB operator (pdf 150)] of Olson et al. (1986) and [RTSA convergence acceleration (pdf 150)] of Ng (1974).

³⁰ MULTI extension to 3D parallel computation using short characteristics with further-away contributions corrected by iteration.

steep horizontal gradients are similarly important in 3D radiative transfer. Steep horizontal gradients occur for example already in the photosphere in and above granulation and magnetic concentrations constituting network and plage. Obviously they occur in and around the multitude of small dynamic structures constituting the higher atmosphere.

4. LTE: Holweger models

The classic Holweger models³¹ (Holweger 1967 and HOLMUL of Holweger & Müller 1974) were a pinnacle of solar LTE interpretation. They replaced curve of growth³² abundance determination by numerical abundance determination. They ignore the existence of the solar chromosphere to avoid self-reversals in strong optical lines³³, but nevertheless HOLMUL became highly popular³⁴ with abundance determiners because it worked so well, giving them smaller spread for multiple lines than other standard models. No wonder because the model was made as best fit to photospheric lines, in particular of Fe I, so that fitting similar lines with the model was a self-fulfilling prophecy, in particular for the then much debated Fe abundance itself (e.g., Kostik et al. 1996). Earlier Rutten & Kostik (1982) showed that such model production is also self-correcting through “NLTE masking”: for a steep outward temperature decline the outward increasing ultraviolet $J > B$ excess from scattering and Λ results

³¹ Spectrum synthesis: with the ALGOL program of Baschek et al. (1966) impose a $T(h)$ “model” relation, evaluate density stratifications for the given element mix by assuming hydrostatic equilibrium [RTSA Sect. 7.2.3 (pdf 166)], compute continuum extinction from H^- , extinction of a given line per SB ($b_u = b_l = 1$) in [RTSA Eq. 9.6 (pdf 224)], and integrate the transport equation to obtain the emergent profile of which Holweger used the area (“equivalent width” [RTSA Sect. 9.1.2 (pdf 224)]) as quality gauge, did so for many optical lines and derived a best-fit temperature stratification by trial-and-error. Most analyses of this type (a large “abundance determination” industry during decades) employed critical ad-hoc adjustment parameters: fake line broadening for duplicating observed line broadening with “microturbulence” (adding height-dependence as in Fig. 11 (pdf 18) of Vernazza et al. 1981) and “macroturbulence” (adding anisotropy as in Gray 1977), and fake wing extension with a collisional damping “enhancement factor”.

³² Treated in practical SSA 3 (pdf 28). Figure 4 (pdf 6) of Rutten & Zwaan (1983) may have been the last solar Fe I one.

³³ As in the dark Na I D lines treated in practical SSB 3 (pdf 22) but also in the strong Fe I lines that Holweger employed. Their absence was attributed correctly to NLTE scattering by others but Holweger insisted persistently that NLTE computer programs fatally overestimate NLTE departures by not including sufficient hydrogen-atom collisions. When he refereed Carlsson et al. (1992) explaining the enigmatic Mg I emission lines at 12 micron this was also his main complaint, but the Rydberg recombination modeled there was already collision-dominated. The formation of these striking features is interesting because it combines NLW photon pumping (photo-ionization), NLW photon suction (recombination driven by strong-line photon loss) and a diffusive radiative-collisional Rydberg population departure flow. See the cartoon explanations in Rutten & Carlsson (1994) including Mats’ “Rydberg flows for kayakers” in Fig. 4 (pdf 7) (better quality here). Actually, Lemke & Holweger (1987) had come close to model these emission lines properly except that their Mg I model atom did not reach high enough. Their paper was wildly and wrongly attacked by Zirin & Popp (1989), in turn severely rebutted by me in Carlsson et al. (1992). This impressed Zirin so much that he saw me as potential successor. I saw him as thin because in the abstract he stated that these Mg I lines are thin. They are not in his sense, but that itself is a no-no because lines cannot be thin (some width threshold in Å?). A solar-atmosphere structure can be thin or thick or effectively thick in a line (maybe the Sun is thin in neutrino lines). Never say “this line is thin” or earn my scorn!

³⁴ ADS shows 900+ citations but rate declining since 2009.

in much NLW-type NLTE overionization of minority-species metals [SSF (pdf 111)]. Instead adopting Saha ionization then puts the height assigned to $\tau = 1$ too high so that the fitted temperature gradient gets too shallow and the same as for locations with less steep temperature decline (cartoon scheme in Fig. 4 (pdf 14) of Rutten 1988). Different surface structures with different actual gradients (as granules and lanes) can then still be fitted by a single shallow gradient.

So-called “inversion” codes (I find “best-fit” better suited) are automated versions of Holweger’s trial-and-error model derivation procedure³⁵. Copying Holweger’s fads also brings the fallacies including NLTE masking, an important failure because NLTE scattering in the ultraviolet bound-free edges controls the opacity of minority-species atomic lines throughout the spectrum. While in the optical these often have source functions close to LTE (maintained by stronger multiplet members in the ultraviolet) their opacities have NLTE deficits up to an order of magnitude from ultraviolet overionization set by steep vertical and horizontal temperature gradients in deeper layers. The prime example is Mg I 4571 Å which is a forbidden transition and therefore has $S = B$ up to large height but suffers considerable extinction NLTE even in 1D modeling [SSX (pdf 82)], but the same holds for most other optical atomic lines including the Fe I polarimetry pair at 6303 Å [SSX (pdf 83)]. This fallacy has been long ignored but was at last addressed by Smitha et al. (2020). Worse: in the actual 3D solar photosphere matter and radiation gradients also act horizontally, requiring 3D line synthesis (cf. Smitha et al. 2021). Proper quantification of such ultraviolet extinction control is severely hampered by the dense ultraviolet line haze with its own NLTE properties (Fig. 10 (pdf 18) of Rutten 2019). Stronger lines need NLTE modeling not only for their extinction but also for their source function set by their own scattering or by non-2-level detour transitions. When inversion codes are proudly advertised as NLTE usually only the modeled-line resonance scattering is meant, not the extinction-affecting scattering in the bound-free continua nor resonance scattering in the line haze affecting those.

Holweger’s assumptions of 1D modeling, LTE and no chromosphere were also revived in SATIRE irradiance modeling for network and plage (Unruh et al. 1999) which therefore suffers similarly from mistreating the opacity-affecting NLTE ultraviolet continua and their NLTE line haze. More explanation in Sect. 4 (pdf 11) of Rutten (2019).

The Asplund revolution (Asplund et al. 2009, 5000+ citations and steepening) ended the HOLMUL popularity, not so much as an LTE dismissal but by including granulation (Nordlund et al. 2009). Its main effect is that its temperature inhomogeneity upsets the notion that spatially-averaged intensity may be modeled as spatially-averaged temperature because at optical and shorter wavelengths this notion is undone by the Wien non-linearity of the Planck function (Uitenbroek & Criscuoli 2011). In addition simulated granulation undid the “microturbulent” faking, and better atomic physics (Barklem et al. 2000) undid the “damping enhancement” faking.

³⁵ They often apply the further simplification of assuming Milne-Eddington line formation, i.e., constancy of the line-to-continuum extinction ratio with height. This assumption was tested with a MURaM simulation and LTE line synthesis for comparable weak Fe I lines at different excitation energy in Fig. 8 (pdf 10) of Vitas et al. 2009. It is bad at low excitation, better at higher excitation.

5. NLS: Auer & Mihalas modeling

NLS is the realm of 2-level modeling treated extensively in [RTSA Chapt. 4 (pdf 95)], numerical developments around the Λ operator summarized in [RTSA Chapt. 5 (pdf 133)], and numerical PRD formalisms (not yet in RTSA). [SSF (pdf 111)] shows a cartoon summary also discussed in Sect. 4 (pdf 11) of Rutten (2019). Non-local scattering makes J depart from B in setting S according to Eqs. 2 and 3, for bound-free continua and for lines of increasing strength (or different parts of strong PRD lines). The ultraviolet continua gain $\Lambda S \approx J$ excess over the photospheric B decline [SSF (pdf 86)]. Strong lines obtain low S per Λ from $\sqrt{\epsilon}$ scattering by seeing actual temperature gradients as near-isothermal from τ scale compression [SSF (pdf 85)].

I advertise the classic warm-star HI analyses of Auer & Mihalas (1969a, 1969b) here. They were an early pinnacle of 2-level modeling³⁶. Not purely 2-level since adding the HI continuum level and so including the Lyman and Balmer continua to Ly α in the first paper and to H α in the second. The great didactic value of their results is that the effects of these transitions are well separated in height. “Big whopper” [RTSA exercise12 (pdf 254)] poses five pages of hard questions on their graphs that I challenge you to answer³⁷. The hardest is to understand: “Amazingly, the photon losses in the subordinate Balmer- α line, located in the low-energy red part of the spectrum, cause heating of the whole outer atmosphere of this hot star.” [RTSA (pdf 189)]. Because their graphs did not include J we did a multi-level re-do including S , B , J and radiative heating/cooling graphs in Wiersma et al. (2003), giving as answer: “The photon losses in Ba α suck population from the proton reservoir through a collisionally-dominated Rydberg recombination flow and so boost the outward temperature rise.” (pdf 7). All yours to understand.

6. NLS+NLW: Avrett models

The various Avrett models³⁸ (VALIIM of Vernazza et al. 1976, VALIIC of Vernazza et al. 1981, MACKKL of Maltby et al. (1986), FALC of Fontenla et al. 1993 and ALC7 of Avrett & Loeser 2008) are all classic pinnacles of plane-parallel (1D) NLTE modeling (2100+ citations and steepening for VALIIC). Practical SSB 1 (pdf 5) dissects the FALC stratifications with comparison to our own atmosphere which is transparent to sunlight by missing H $^-$ (did you miss it?) treated in the continuum part of SSI and in practical SSB 2 (pdf 13).

SSB 3 (pdf 22) makes you synthesize the Na I D lines from FALC assuming LTE and hence misrepresenting their cores.

NLW was still lacking in VALIIM which only accounted for scattering in the Si I continuum so that its Fig. 23 (pdf 38) multi-page analogon to multi-page VALIII Fig. 36 (pdf 33) shows erroneous $S_\nu \approx B_\nu$ above the Si I threshold at 1682 Å where other electron-donor bound-free contributions dominate. This was remedied in VALIIC but overestimating their effect because not enough line-haze blending lines were included, resulting in a too steep upper-photosphere temperature decline. Including more and more lines from the Kurucz tabulations then brought the upper-photosphere back up in MACKKL and since then it has remained the same. It is remarkably similar to HOLMUL and even to Kurucz or Uppsala radiative-equilibrium models [RTSA Fig. 7.3 (pdf 169)]. The reason is that the upper photosphere is the most homogeneous domain of all. The granular convection has stopped whereas waves (primarily acoustic) do not yet shock. Magnetic fields are still mostly confined to slender fluxtubes at small density in the modeled “quiet” areas. Indeed, more modern Bifrost simulations obtain about the same average temperature decay with relatively small spread at these heights [SSX (pdf 59)].

³⁶ I wonder what Unsöld, who at Kiel had told Holweger to produce a thesis proving that LTE suits the solar spectrum, made of these. In 1967 he wrote to Minnaert that Holweger had indeed definitely proven the LTE veracity of the solar spectrum, in a recommendation for the Bilderberg Conference described in Rutten (2002) (group photo including Holweger (pdf 4)). The Auer–Mihalas results upset his “Physik der Sternatmosphären” (Unsöld 1955, 900+ citations) which was translated by Hans Panovsky and Keith Pierce but never printed because Unsöld insisted that any astrophysicist should learn German to read his book.

³⁷ Spoiler: my answers to most RTSA problems including this one.

³⁸ Spectrum synthesis: PANDORA (Avrett & Loeser 1992) is similar to Holweger’s code in applying hydrostatic equilibrium to a trial $T(h)$ temperature stratification but uses SE NLTE for radiation evaluation in a giant “equivalent two-level” iteration loop treating each bound-bound or bound-free transition that is explicitly taken into account (not added as background opacity) with two-level rate equations, letting iteration take care of multi-level crosstalk. Whereas Holweger concentrated on fitting observed optical lines, most from Fe I, Avrett concentrated on fitting observed disk-center continua, especially in the ultraviolet. These are affected by line crowding (the “veiling line haze” of Labs & Neckel 1972 and Greve & Zwaan 1980) so that Avrett added increasing numbers of lines from the list of Kurucz (2009) and treated them with an imposed ad-hoc gradual source function transition from $S = B$ in the model photosphere to $S = J$ in the model chromosphere to avoid non-observed core reversals that occur in LTE sampling above the temperature minimum (page 243 ff. (pdf 15) of Avrett & Loeser 2008). The line haze was most comprehensively handled brute force in Fontenla et al. (2015) by solving NLTE population equations for very many transitions, doable only in single-shot 1D modeling. Fontenla diverged from Avrett after Fontenla et al. (1993), writing a PANDORA alternative and adding tricks to enhance output similarity to the non-1D non-static non-SE spectra of the actual Sun. First he invoked the Farley–Buneman instability to warrant adding ad-hoc artificial pressure (the Avrett stars use observed microturbulence for turbulent pressure); later he mucked gravity ad-hoc to extend the model chromosphere to reproduce CO lines that probably have 3D(t) NLT formation (Uitenbroek 2000). I prefer the ALC7 star of Avrett & Loeser (2008) for my spectrum-formation demonstrations [SSX (pdf 72)]–[SSX (pdf 140)]. It isn’t the Sun but it is self-consistent within its RTSA physics and well-suited to showcase this physics.. PANDORA is web-available but documented only in many pages of coding requests and specifications (including Fortran variable names) to Rudolf Loeser that reside in Avrett’s CfA office (Petr Heinzel holds copies in Ondrejov).

I love the Avrett models, in particular VALIIC because of the many diagrams in Vernazza et al. (1981) and especially its many-page Fig. 36 (pdf 33) continuum formation diagrams (some copied in [RTSA (pdf 204)]–[RTSA (pdf 206)]). Since VALIIC obeys all the standard RT equations, meaning all those in RTSA, these graphs describing spectral features arising from the VALIIC density and temperature stratifications provide valuable insights on spectrum formation and its intricacies. They are of enormous didactic value because *everything* in Avrett’s output graphs is fully understandable from the input physics \approx RTSA physics. The same holds for the newer Avrett models and his latest ALC7. Therefore I added many analogous ALC7 figures to SSX: [SSX (pdf 73)] showing ALC7 stratifications, [SSX (pdf 76)] ultraviolet continua, [SSX (pdf 77)] hydrogen line formation, [SSX (pdf 77)] overview of strong-line formation, then [SSX (pdf 78)]–[SSX (pdf 81)] explaining my triple line-formation plot formats using Na I D₁ and then followed by such triple formation plots for thirteen lines in [SSX (pdf 82)]–[SSX (pdf 94)]. They were all made³⁹ with the 1D version of the github-public RH code⁴⁰ of Uitenbroek (2001). They represent a detailed view of how all these lines form in the ALC7 atmosphere. Any student of thick solar spectrum formation should be able to understand and appreciate all these curves in full detail. I invite you to study and explain:

- N_e stratification;
- Eddington-Barbier validity in all lines;
- PRD-split source functions of Ba II 4554, Ca II K, Mg II k, Ly α ;
- thermalization depth for all lines, in particular H α ;
- NLTE extinction dip of Mg I 4571, Fe I 6301.5, Mg I b₂ but not for Na I D₁, He I 10830;
- LTE extinction of Mg II k, H α , H β , He I 584;
- slight rise in NLTE over-extinction for Ly α .

However – the stern caveat is that I love the Avrett models only for representing unrealistic non-existing virtual didactic stars (I call ALC7 “the ALC7 star”). These stars are plane-parallel (1D) without inhomogeneities or magnetism or any sort of waves or any type of reconnection – no granules, spicules, floccules or whatever else making solar physics non-plane-parallel interesting. The Avrett models are a marvelous boon to an RT teacher like me, but they have detrimental effects on far too many colleagues who accept their stratifications as a valid average over small fluctuations around a realistic physical mean and who mistakenly regard their spectrum formation details as valid for their own solar diagnostics. VALIIC Fig. 1 (pdf 3) is undoubtedly the most-shown figure in all solar physics but probably also the most misinterpreted.

³⁹ Using IDL. All my IDL programs are website-available at [Recipes for IDL](#). The RH plot programs in [rplib](#), LTE line formation programs in [ltelib](#), SDO alignment pipeline in [sdolib](#), SST data-handling programs in [sstlib](#), versatile image sequence browser [showex](#) in [imagelib](#), etc. Installation is described in [this manual](#). I even have an IDL manual.

⁴⁰ Spectrum synthesis: RH is named after Rybicki & Hummer (1992) and follows their scheme of multi-level approximate lambda iteration [RTSA Sect. 5.3.2 (pdf 145)], not iterating Λ for J_ν but the Ψ operator for j_ν . It permits overlapping lines, includes PRD and full-Stokes options, exists in 1D, 2D, 3D, spherical, and Cartesian versions, and more recently also in parallel multi-column “1.5D” (Pereira & Uitenbroek 2015). I used RH 1D version-2 with H, He, Si, Al, Mg, Fe, Ca, Na, and Ba active, C, N, O, S, and Ni passive, and with 20 mÅ sampling of 343 000 lines between 1000 and 8000 Å in the atomic and molecular line list of Kurucz (2009). Figure 6 (pdf 13) of Rutten (2019) gives an overview of their extinction in the FALC star. The line haze is prominent between $\log \lambda = 3$ and 4.

Take H α as example. In VALIIC Fig. 1 (pdf 3) Avrett, admirably careful, drew its core coming from the VALIIC chromosphere, its wing from the low VALIIC photosphere with an extended gap in between that is not present in his formation spans of Ca II K and Mg II k. He did so because at low temperature the Boltzmann excitation and therefore the extinction of H α are negligible⁴¹. But the actual H α core in actual quiet Sun mostly samples fibril canopies that reach higher than the entire VALIIC model.

Worse, the VALIIC chromosphere and similar Avrett chromospheres do not portray average fibril temperatures but ultraviolet radiation-temperature maxima reached in acoustic shocks in internetwork regions underneath H α fibril canopies. These radiation temperatures are Wien-weighted to the shock maxima and not linear temperature averages. This was shown already in Fig. 4 (pdf 8) of Carlsson & Stein (1994) with the demonstration in Fig. 5 (pdf 11) that the nonlinear Wien weighting skews the apparent average to an Avrett-type apparent chromosphere, along with their marvelous RADYN reproduction of actual internetwork shocks observed by Lites et al. (1993) in Fig. 14 (pdf 23). These well-known results were formally published in Carlsson & Stein (1995) and Carlsson & Stein (1997).

Figures 8–12 (pdf 16) of Carlsson & Stein (1994) also introduced the informative Carlsson four-panel spectral-feature breakdown graphs⁴². They clearly demonstrate the importance of NLT effects even though the spectral synthesis assumed SE. The observed bright Ca II H_{2V} grains (reviewed in Rutten & Uitenbroek 1991) which the simulation reproduced so admirably exist only because previous shocks define the opacity distribution along the line of sight. The bright grain represents an upward traveling acoustic wave at too low height to show shock heating; its bright visibility is defined by higher-up downdraft after the passage of an earlier wave that shocked higher up.

In AIA 1700 and 1600 Å movies these waves in quiet internetwork regions stand out as fast-moving fast-evolving wisps of emissivity amid stable network evident as bright grains representing kilogauss “fluxtube” magnetic concentrations. The internetwork wisps represent upward propagating waves excited by the photospheric p -mode interference pattern. The 1600 Å images sample them slightly higher because the summed photoionization extinction of electron donors Mg I, Fe I, Si I, and Al I increases for shorter wavelength (VALIIC Fig. 36 (pdf 33 ff)). This increase produces the Fourier phase differences in the upper

⁴¹ See dashed curve in the first panel of [SSX (pdf 92)]. Observationally the gap is evident when you shift the SST/CRISP H α passband from line center to a wing for a quiet-Sun target. Up to about $\Delta\lambda = \pm 0.5$ Å the scene usually shows fibrils extending from network and then you suddenly drop into deep-photosphere granulation, skipping the middle and upper photosphere. Only in rare utterly quiet areas you may see somewhat higher-up reversed granulation near $\Delta\lambda = \pm 0.5$ Å. I offer two SST examples. The first is a very quiet target corner in the data of Roupe van der Voort et al. (2007) in [this Ca II H + H \$\alpha\$ blue-wing movie](#) where reversed H α at $\Delta\lambda = -0.45$ Å shows reversed granulation as grey background pancakes. The second is a similarly very quiet target (in a disk-center coronal hole) that you may inspect yourself by doing my [practical on SDO–SST co-alignment](#) enabling blinking against reversed granulation in Ca II 8542 Å.

⁴² One shown in [SSX (pdf 156)], four in Figs. 4 (pdf 5)–7 (pdf 8) of Carlsson & Stein (1997). I strongly recommend studying these (by understanding them you join a select club). In my courses they became examination material. An astute student noted that the second panel of [SSX (pdf 156)] exhibits the wrong assumption of CRD. Carlsson and Stein argued that their neglect of Ca II H PRD was compensated by not including Mg II h & k.

panel of Fig. 18 (pdf 18) of Krijger et al. (2001) reproduced per RADYN simulation by Fossum & Carlsson (2005b)⁴³.

The magnetic concentrations outlining network appear with brighter contrast at 1600 Å than at 1700 Å. Plane-parallel colleagues attribute this enhancement also to increased donor-ionization opacity and standard “network” and “plage” models therefore have less steep upper-photosphere temperature decay than their “quiet” companions for internetwork. However, the actual fluxtube brightness is photospheric hole-in-the-surface radiation, with deeper holes at shorter wavelength. This is also known for decades; I recently wrote a review as caption to Fig. 75 (pdf 90) of Rutten (2020) and refer to that. Actual magnetic concentrations are close to radiative equilibrium throughout the photosphere without evidence of kinetic heating as expected for structures that inhibit convection (Fig. 7 (pdf 7) of Sheminova et al. 2005).

Thus, the standard-model “chromospheres” non-linearly represent under-the-chromosphere internetwork shocks⁴⁴ plus misinterpreted network surface holes. Nothing to do with the on-disk chromosphere in H α that carries the name originally given by Lockyer (1868)⁴⁵ % Rutten vienna irradiance for the colorful off-limb appearance of the Balmer lines and He I D₃.

Yet worse, actual H α canopies in quiet areas are mostly made by spicules-II (more below). These are seen as outer-wing RBE (Roupe van der Voort et al. 2009) and RRE (Sekse et al. 2013) darkening that reach heights around 7000 km (Pereira et al. 2014) far above any standard model. So much for ascribing outer-wing intensities to deep-photosphere sampling and so much for equating heating with brightness – they heat to EUV visibility (Henriques et al. 2016) but are dark.

Yet worse, there even exist publications that used VALIIC Fig. 1 (pdf 3) to define the “height difference” between e.g., Ca II K₃ and the core of H α to identify and measure wave propagation and explain coronal heating. Maybe there exist plane-parallel stars in a parallel plane universe where this is a viable tactic (but do those have coronae?)

⁴³ Who also laid the long-debated attribution of coronal heating to acoustic waves to rest in Fossum & Carlsson (2005a), but unfortunately with what I call a “silly” publisher not furnishing a direct pdf opener on ADS. Page linking such publications (e.g., *Solar Physics* since Springer bought Kluwer) presents a multi-click hassle. If your remote library offers *Lean Library* its browser app may reduce this, but I avoid page-linking silly publications. (If you publish in *Solar Physics* you should always add an arXiv upload and ignore Springer’s stipulations against that – see my *Springer nasturtiums*.) Fortunately, they also wrote directly-opening Fossum & Carlsson (2006) on this topic. A previous directly-opening alternative in coronal heating by waves is Whitaker (1963) who (with Parker’s blessing well before nanoflares) proposed gravity waves as main heater and in his Fig. 1 (pdf 4) introduced the “diagnostic” k - ω diagram in solar physics (from Hines 1960 geophysics, see my *p-mode history lecture*). The k - ω diagrams in Fig. 3 (pdf 3) of Rutten & Krijger (2003) exhibit gravity-wave power and phase difference signatures but I doubt that gravity waves heat the corona (but see Straus et al. 2008).

⁴⁴ A domain I called “clapotsphere” in Fig. 12 (pdf 7) of Rutten (1995).

⁴⁵ I typed the report on Lockyer’s presentation into ADS, remain its main citer so far, and look forward to write “less refrangible” in publications [SSX (pdf 12)] – [SSX (pdf 14)]. Lockyer’s total of about 50 ADS citations (but reads steepening) shows how citation rating utterly fails for the first professor in solar physics and the founding editor (for 50 years!) of *Nature*. Worse: I am not aware of a sound explanation why his He I D₃ is so extraordinary strong off-limb where it ranks between H γ and H β in brightness and off-limb extent, but is nearly invisible on the disk whereas the Balmer lines are also strong features there (Fig. 10 (pdf 18) of Rutten 2019).

7. NLS+NLW+NLT: Oslo simulations

NLT is the current frontier in solar spectrum interpretation, not just in underlying MHD phenomena as the Carlsson-Stein shocks but by also not assuming SE in spectrum synthesis. Anything you see may not be so much how it appears now but rather what it was before. Outdoors example: airliner contrails on our sky signify that aircraft engines passed before. If you don’t know that aircraft exist you may have a problem to explain white clouds appearing in long lines.

The key publications I summarize here are the 1D(t) HD RADYN analysis of acoustic shocks by Carlsson & Stein (2002) and the 2D(t) MHD Stagger simulation of network and internetwork shocks by Leenaarts et al. (2007). The first showcases the physics, the second demonstrates the effects. Neither includes spectrum synthesis but the hydrogen rate analyses of the first and the hydrogen population results of the second suffice to designate these publications classics.

Carlsson & Stein (2002) presented a careful and illuminating analysis of hydrogen partitioning in acoustic shocks as those of Carlsson & Stein (1997). Key results are summarized in [SSX (pdf 165)]. The main agent is Ly α . They found that detailed radiative balance is generally a close approximation for Ly α , in agreement with the discussion on VALIII p. 662 (pdf 29): about as many photons go up as down, very many more than collisions up or down. Most photons are created per pair **d** but then resonance scatter very many times without coming far because their mean free path is small (1 cm in the middle row of Fig. 1 (pdf 4) of Rutten 2017b) with scattering thermalization length about 10 km [SSX (pdf 90)] due to the immense $n_1 \approx N_H$ density while the probabilities of destruction **a** and Balmer detour **h** are small [SSX (pdf 90)]. This approximation was imposed as input by Leenaarts et al. (2007) to avoid quantifying large numbers that effectively cancel.

Figure 3 (pdf 4) of Carlsson & Stein (2002), reproduced in the [SSX (pdf 165)] summary, illustrates this Ly α photon balancing as negligible net 1-2 rate. The fat transitions there (large net photon rate) are photo-ionization in the Balmer continuum and recombination with $\Delta n = 1$ steps⁴⁶ ending with fat H α . For given n_2 population (highly non-E in post-shock cooling) this loop obeys SE but it is far out of LTE because the impinging Balmer continuum originates in the deep photosphere, with radiation temperature about 5300 K [SSX (pdf 76)]. Where this value exceeds the local temperature “photon pumping” enhances ionization. There are also contributing photon losses in heavily scattering H α [SSX (pdf 91)] which operates within the low-energy 3.6 eV hydrogen top as a “photon suction” alkali resonance line (Bruels et al. 1992; explanation with Fig. 2 (pdf 4) in Rutten & Carlsson 1994.)

The key hydrogen balance for NLT is the Ly α collision balance. The collisional up and down rates differ much in temperature sensitivity by being set by the Boltzmann ratio in the Einstein up-down relations [SSX (pdf 166)] [RTSA p. 23 (pdf 43)] [RTSA Sect. 3.2.5 (pdf 70)]. They determine the settling time scale at which Ly α reaches Boltzmann equilibrium. A few cases are plotted in Fig. 6 (pdf 7) of Carlsson & Stein (2002), reproduced in [SSX (pdf 166)]. In hot shocks the frequent Ly α up- and down collisions make the balance reach Boltzmann equilibrium in seconds, but in subsequent post-shock cooling gas the settling time scale increases to multiple or many minutes. During this time the large n_2 overpopulation also governs large non-E overionization since the whole top of the hydrogen atom including

⁴⁶ The “Rydberg ladder” produces HI emission lines in the infrared (Carlsson & Rutten 1992).

the proton population is defined by this lower boundary condition. The Balmer-top SE loop just adds yet more overionization if the temperature drops below 5300 K.

The next step in non-E simulation was Leenaarts et al. (2007), going from 1D to 2D and from HD to MHD. [SSX (pdf 167)] is a summary. The three panels at its top are cutouts showing three of the nine quantities in Fig. 1 (pdf 4) at a sample time step. They demonstrate that the simulation (evolved after starting from an LTE initializing simulation) portrays a quiet solar scene with two opposite-polarity magnetic concentrations 8 Mm apart that resemble network fluxtubes, with internetwork in between showing a canopy-like dome with cool to very cool gas underneath and less steep upward density decay. For me the small 9-panel thumbnail underneath in [SSX (pdf 167)] is a clicker that opens [this movie version](#) running the whole simulation. Please download and play it. It vividly shows how shocks (thin blue filaments in temperature) travel up along the field concentrations and more erratic between them, the latter kicking up the apparent canopy. The first represent field-guided dynamic fibrils as evident from their characteristic time-slice parabolas in the lefthand column of Fig. 3 (pdf 6). The internetwork shocks are acoustic Carlsson-Stein shocks.

The last panel of the three in [SSX (pdf 167)] and the nine in Fig. 1 (pdf 4) and its movie version show the NLTE departure coefficient b_2 of HI level $n = 2$, upper level of Ly α and lower level of H α ⁴⁷. Its variations are enormous, reaching values up to 10^{12} in cooling post-shock blobs⁴⁸. This is not NLTE at the 0.1-1 dex level traditionally important in solar and stellar abundance studies – this is 12 dex! The next to last panel of Fig. 1 (pdf 4) and its movie version shows the departure for the HI continuum level ($n = 6$ in the atom model) and illustrates that Balmer continuum pumping adds up to another 3 dex for the coolest clouds.

Figure 2 (pdf 5) of Leenaarts et al. (2007) is also best studied in its [movie version](#). Its panels show behavior of the y -axis quantity along the dotted vertical lines in the fourth panel of Fig. 1 (pdf 4), at left sampling the lefthand field concentration and at right internetwork. In the lower three rows the thick curves are the simulation results, the thin curves the values obtained by assuming LTE instead so that the curve separations correspond to the departure coefficients in Fig. 1 and its movie version. Playing this movie shows shocks running up with time in the temperature curves in the lefthand top panel. The actual shocks in the Fig. 1 movie tend to go slanted in the internetwork, so that the right-hand column samplings are not along-the-shock path histories⁴⁹

⁴⁷ Be aware that Avrett and Fontenla used the Menzel definition of departure coefficients described in VALIII Eqs. 13 – 18 (pdf 29). I use the more transparent Zwaan definition [RTSA Eq. 2.104 (pdf 53)] and used to write these as β_l and β_u following Wijbenga & Zwaan (1972). Their values reverse for majority species as HI, which led Fontenla et al. (2009) to misinterpret their own results (Rutten & Uitenbroek 2012). Various other authors (not to be named) similarly reversed the meaning of VALIII Fig. 30 (pdf 29) into the b_1 curve implying chromospheric hydrogen ground-state population ten times the local gas density.

⁴⁸ This panel also shows high-up green arches. I think that these are artifacts stemming from the input tractability assumption that Ly α obeys detailed radiative balance.

⁴⁹ When Mats Carlsson hunted in the data of Lites et al. (1993) he found only few pixels with nice multi-cycle spectrum-versus-time behavior as in RADYN output and selected the best for Fig. 18 (pdf 13) of Carlsson & Stein (1997). Others as the two less matching samplings in their Fig. 17 (pdf 20) may have been too slanted to produce vertical-column NLT signature or had too much sideways wave interference. Their four samplings are marked in the observed time slices in Fig. 2 (pdf 4) of Rutten et al. (2008) where the rightmost panel shows slanted propagation tracks crossing the latter two (149 and 30). The very quiet-target SST

but represent different shocks at different times. The movie strikingly demonstrates that the ionization fraction, proton density and n_2 population density in the lower rows reach LTE values in shocks but thereafter do not drop steeply along with the temperature. Instead they hang roughly at the value they got in the shock. There should be eventual settling to the LTE value, but long before that the next shock arrives: shocks repeat faster than the settling time scale.

The second row shows that hydrogen generally does not ionize fully in the shocks but only a few percent. However, this already means two orders of magnitude increase of the electron density which in neutral-hydrogen gas sits at the 10^{-4} abundance fraction of the electron donor metals (VALIII 47 (pdf 67) [SSX (pdf 72)]). This increase in collision frequency appears sufficient to obtain LTE Boltzmann equilibrium in Ly α giving LTE Balmer extinction. Another condition for this equilibrating is that a feature should be thick enough to contain Ly α , optically thicker than the thermalization length from its surface [SSX (pdf 90)]. At percent-level ionization hydrogen retains sufficient n_1 opacity to keep these shocks effectively thick.

Since these classic simulations the Oslo simulators went to 3D(t) MHD Bifrost of Gudiksen et al. (2011) [SSX (pdf 159)]. Reference lists (until 2018 at the time of writing) are given in [SSX (pdf 160)] – [SSX (pdf 163)]⁵⁰; many studies employ the public snapshot of Carlsson et al. (2016). The Bifrost stars are far more solar-like than the Avrett stars by being 3D(t) with motions and magnetism. Unlike the Avrett stars they contain realistic granulation, acoustic waves and shocks, magnetic concentrations arranged in network patterns, dynamic fibrils, bipolar-network-connecting chromospheric fibrils, and Ellerman bombs. However, they still lack in spicules-II and attendant fibrils around network as major quiet-chromosphere agents, and their cube shapes are yet too small for supergranulation, active regions, and larger-scale coronal fine structure. Bifrost spectral synthesis has mostly concentrated on the IRIS diagnostics. Obviously it beats Avrett-star spectral synthesis in NLS, although most analyses rely for tractability on columnar modeling with the RH 1.5D code of Pereira & Uitenbroek (2015). The Avrett stars handle NLW better with respect to ultraviolet ionization and the problematic ultraviolet line haze (Fig. 10 (pdf 18) of Rutten 2019). Various Bifrost runs included NLT for hydrogen (as in the classics above), but not in subsequent spectral synthesis⁵¹.

8. NLS – NLW – NLT chromosphere spectrum

SE is usually a sound assumption for thick spectral modeling of photospheric structures (SE NLTE) and for thin spectral modeling of coronal structures (SE CE). Chromospheric structures

movie linked in footnote 41 and [here again](#) shows fast-varying threads of H α “mushroom” bomb shells following on and around Ca II H $_{2V}$ grains, indeed not radial along the line of sight: internetwork shocks are 3D(t) rather than 1D or 2D phenomena. Per-pixel Fourier analysis to establish vertical phase relations makes no sense for these. The cadence of the movie is 7 seconds but faster is clearly desirable. My [SDO-SST alignment practical](#) also shows these H α mushrooms in the upper-left quiet corner of the SST field but at slower cadence.

⁵⁰ ADS abstract search “Bifrost” and “solar” gives publication count and Hirsch $N = 77$, $h = 17$, solidly enough for a solid permanent position. “MURaM” and “solar” $N = 74$, $h = 19$ idem for the MHD simulation code of Vögler et al. (2005). Maybe you should simulate – so it goes.

⁵¹ But see Golding et al. (2017) for an analysis of EUV helium lines.

in between are the hardest to model because NLT reigns next to NLS and NLW in making them cycle through thick and thin⁵².

Let's start with quiet Sun. In AIA images the quiet-area chromosphere has two major constituents: (1) heated chromosphere, visible in 304 Å and 131 Å everywhere around network and qua surface patterns cospatial with the fibrillar H α chromosphere (Appendix B (pdf 11) of Rutten 2020), and (2) coronal bright points, best seen in 193 Å images as small ensembles of EUV-bright loops located at and connecting bipolar network (review by Madjarska 2019)⁵³.

Both constituents consist of small dynamic features occurring with fast repetivity. The heated-chromosphere agents are spicules-II ejected from network and observed as RBEs (Roupe van der Voort et al. 2009) and RREs (Sekse et al. 2013) with gas heating to EUV visibility (Henriques et al. 2016) well beyond the shock heating of Carlsson & Stein (2002) and Leenaarts et al. (2007). The spicule-II aftermaths of cooling recombining return flows then cause the dark H α -core fibrils around network known as "mottles" in older days, a few minutes later with their H α opacities probably much enhanced by NLTE cool-down retardance as in the post-shock clouds of Leenaarts et al. (2007). Evidence are the time-delay darkest-darkest correlations⁵⁴ in Rutten et al. (2019).

Sparser (but not rare) coronal bright points are probably heated by reconnection near the loop tops with subsequent heating of their chromospheric footpoints (Madjarska et al. 2021), likely by particle beams (Frogner et al. 2020), cf. Rutten (2020). These features can live fairly long, the smallest⁵⁵ the shortest, but AIA 193 Å movies always show frequent change suggesting continuous renewal.

To reproduce such dynamic nature numerically, even for just "quiet" chromosphere, poses enormous challenges because the MHD simulations must produce spicules-II as copiously as ac-

tual solar network does and must then be combined with 3D(t) NLS–NLW–NLT ("non-E") spectral synthesis including PRD at least for Ly α to recover the observed H α chromosphere, and in addition must produce small-scale bipolar activity causing and governing coronal bright points as observed

ALMA has the potentiality to sample and measure the chromosphere sharper and faster than DKIST. Plane-parallel modeling and various simulations have suggested that ALMA samples the upper photosphere dominated by acoustic waves on their way to become shocks, but these efforts erred in assuming SE. Because Ly α -controlled NLT opacity enhancement of the HI n_2 population also gives enhanced hydrogen ionization I have instead predicted that NLT-opaque H α canopies are similarly NLT-opaque in the HI free-free continua sampled by ALMA (Rutten 2017b with a tutorial in Rutten 2017a)⁵⁶. This means that, while ALMA is a thermometer thanks to free-free source function LTE, it more likely samples H α canopy fibrils than internetwork shocks underneath thanks to NLT extinction NLTE – a blessing because we understand internetwork shocks for decades but do not understand the chromosphere. The good correlation between ALMA intensity and H α width (both gauges of temperature as shown by Cauzzi et al. 2009) found by Molnar et al. (2019) confirms this view⁵⁷.

There have been and there are efforts (e.g., Eklund et al. 2021) to synthesize ALMA signatures of clapotospheric undercanopy shocks from the public Bifrost simulation of Carlsson et al. (2016) but since this simulation does not show spicules-II nor attendant H α canopy fibrils emanating outward from its network such efforts apply likely best or only to very quiet areas as the ones offered in footnote 41. AIA 304 Å images can assist in locating such canopy-free locations. They are rare. Elsewhere my hope is that ALMA will help solve the long-standing problem of chromospheric heating in quiet areas. Hopefully soon so that we can turn to activity in its current upswing to maximum.

For active-Sun chromosphere phenomena I refer to Jongchul Chae's contribution in this workshop because I have not worked on these⁵⁸ – but as appetizer I link to the active-region scenes in

⁵² I skip the so-called "transition region" because I don't think such exists as a separable domain in the solar atmosphere. The shocks in the Fig 1 movie of Leenaarts et al. (2007) lift the corona above them tremendously up and down, with a steep space-time-varying temperature jump as instantaneous envelope but not a global shell as in standard models. The simulated corona there reaches lower in the magnetic concentrations, as it does in "moss" in denser plage regions. Furthermore, the quiet-Sun chromosphere observed in the "transition" He II 304 Å line with AIA resembles the fibrillar H α chromosphere so well that one may co-align quiet-Sun H α and 304 Å images by pattern correlation, as shown and discussed in Appendix B (pdf 11) of Rutten (2020). This pattern similarity extends even to AIA 131 Å images. The 304 and 131 Å emitting gas around quiet network is not a thin transitional envelope around H α fibrils but represents hot ionization phases, i.e., hot tips of spicules-II and their still hot aftermaths whereas H α fibrils show cooling recombining return gas NLT-darkest near the spicule-II ejecting network. Both outline canopies with similar surface patterns because each samples the quiet chromosphere in successive manifestations. The chromosphere ain't stacked in layers but is NLT unstuck in time (Billy Pilgrim syndrome).

⁵³ For a quick SDO overview inspect and page-blink the 10 "triple" image sets in Figs. 17 (pdf 34)–46 (pdf 63) of Rutten (2020). For each the first is a large-field 193 Å image showing coronal activity, coronal holes, coronal bright points. The second is a clipped "fire detector" multiplication of 304 Å and 131 Å images with grey patches showing heated chromosphere and cyan-colored pixels marking the feet of coronal bright points. The third is the corresponding HMI magnetogram. The 10 triples sample low and high activity and low and high latitude.

⁵⁴ My SDO-SST alignment practical also enables you to inspect such correlations yourself.

⁵⁵ Advertised as newly-discovered Solar Orbiter "campfires" but already described by Falconer et al. (1998).

⁵⁶ Background: RBEs and RREs reach higher degrees of hydrogen ionization than the shocks in the Fig 2 movie of Leenaarts et al. (2007). They extend further in H α than in Ca II 8542 Å (lower-left panel of Fig. 1 (pdf 3) of Sekse et al. 2012) because Ca II ionizes before H I. Where their tips have AIA EUV visibility (Henriques et al. 2016) hydrogen is nearly or fully ionized. The resulting recombining fibrils are also longer in H α than in Ca II 8542 Å (Fig. 3 (pdf 4) of Cauzzi et al. 2009). The few-percent ionization in the shocks in the movie with its two-orders of magnitude electron density increase already suffices to reach near-SB proton densities (3rd movie row). Hence SB proton densities must also occur in spicules-II, warranting the straightforward SB extinction comparisons in Fig. 1 (pdf 4) of Rutten (2017b) for the hot spicule-II phases while recognizing that these high extinction values persist NLT-wise afterwards in the return fibrils constituting opaque canopies while instantaneous SB values drop steeply with temperature.

⁵⁷ Another confirmation that ALMA sees quiet-Sun chromospheric canopies is that quiet-Sun ALMA images can be co-aligned with H α images through cross-correlation, even with bad but always available GONG H α images. Being full-disk these can be precisely co-aligned to AIA 304 and 131 Å images and then serve as ALMA-to-SDO intermediary. I have done this and indeed found pattern correlation between the ALMA and AIA chromospheres.

⁵⁸ Except Ellerman bombs (Watanabe et al. 2011, Rutten et al. 2013, Vissers et al. 2013, Rutten et al. 2015, Vissers et al. 2015, Rutten 2016, Vissers et al. 2019). I suspect that I helped boost interest in Ellerman (1917) so that after half a century of ignorance it shot up in ADS citations, reaching 100 in its centennial year (thus: if your nice discovery remains unnoticed – relax waiting for ADS to revive it). Ellerman bombs

Fig. 2 (pdf 6) of Rutten (2017b) where bright Ly α grains show dynamic heating and dark H α fibrils show NLT cooling. It is amazing how these scenes, both sampling hydrogen atoms, differ in appearance. ALMA samples hydrogen ions and may be able to measure both types of feature at fast enough cadence to establish and correlate cause–effect delays. There may even exist features with sufficient Rydberg-ladder NLT recombination emissivity for visibility in the HI 30- α line at 231.901 GHz, enabling direct measurement of chromospheric Zeeman splitting (Sect. 6 (pdf 13) of Rutten 2017a).

There are also dark filaments in these appetizer scenes suggesting “chromospheric” neutral hydrogen gas in the corona that appears longlived – but AIA 304 Å filament movies always show small fast disturbances running through (cf. Lin et al. 2012) that suggest frequent ionization-recombination cycling with NLT opacity enhancement. ALMA may directly measure such frequent refurbishment. I suspect that it causes and maintains the extraordinary filament visibility in H α and He II 304 Å.

9. Conclusion

Solar radiative transfer modeling has come a long way but it isn't there yet. The physics was well understood by the 1970s – no dark matter nor dark energy in the solar atmosphere⁵⁹. Numerical modeling started about then with the advent of electronic computing which was welcome because analytic theory had reached its limit in Kourganoff (1952). Numerical modeling provided great insights even though initially mostly within the misleading straitjacket of plane-parallel atmospheres. Nowadays the major challenge is to obtain realistic spectrum synthesis from realistic solar-atmosphere simulations to provide guidance to interpret high-quality observations conveying solar truth. Full 3D(t) synthesis of all spectral features for every voxel at all times of a 3D(t) simulation is yet a bridge too far so that the current simulation and synthesis frontier lies in clever shortcuts (reviews by Pereira 2019 and Leenaarts 2020).

Shortcuts as adopting 1.5D columnar synthesis ignoring non-radial matter and radiation gradients, Holweger-style inversion with NLTE masking, neglect of NLTE ultraviolet scattering and neglect of NLT memory by assuming SE may be as misleading

are photospheric but of interest here because the spectral signature of these strong-field reconnection events is complex and instructive. They appear very bright only in the H α wings because the H α line core remains shielded by overlying dark active-region fibrils (Fig. 3 (pdf 4) of Rutten et al. 2013) and they are therefore similarly shielded and invisible for ALMA (prediction 9 (pdf 9) of Rutten 2017b confirmed by da Silva Santos et al. 2020). They are not visible in the Na I D and Mg I b lines (Ellerman 1917, Rutten et al. 2015) because they are hot enough to fully ionize neutral metals and they appear bright in UV continua (AIA 1700 Å and 1600 Å) from Balmer continuum brightening with neutral-atom bound-free opacity ionized away. The cartoon in Fig. 2 (pdf 5) of Rutten (2016) added one to the last panel of Fig. 1 of the simulation of Leenaarts et al. (2007). Because they are hotter and denser than the shocks in which Ly α already reaches collisional equilibrium their H α extinction obeys SB partitioning, permitting the straightforward SB opacity comparisons in Fig. 5 (pdf 9) of Rutten (2016). The actual Ellerman-bomb H α profile under the canopy is probably similar to Mg II k (H α reaches similar extinction and emissivity at high temperature) with a very high peak and a small central dip as in Fig. 4 (pdf 7) of Vissers et al. (2015). Presently the interest has moved to non-active quiet-Sun QSEBs (“quiet-Sun Ellerman-like brightening”) marking ubiquitous but hard-to-detect small-scale photospheric reconnection (Roupe van der Voort et al. 2016, Danilovic 2017, Joshi et al. 2020).

⁵⁹ For a conflicting speculation search ADS with *abs:"axion quark" and "solar orbiter"* – amusing but not to be honored by citation.

as believing plane-parallel standard models – but just as those they may be educational steps along the way.

Every aspect treated here must be considered: the Sun is a beautiful but complex being. We are very fortunate that our star offers such great complexity to keep us on our toes.

Acknowledgements. I thank Ram Ajor Maurya and M.K. Ravi Varma for inviting me to teach. Earlier invitations to teach, in Bandung, Mitaka, Palo Alto, Seoul, La Laguna, Freiburg, Newcastle and Weihai (usually a full week for this material) led to displays SSF and SSX. I hope more will come in a post-covid era. I also thank F. Paletou, J. Leenaarts and T. Pereira for improvements. As always I relied on the splendid ADS library. ADS also instructed me in pdf page opening and kept my older page links active in its 2019 revamp.

References

- Asplund, M., Grevesse, N., Sauval, A. J., & Scott, P. 2009, ARA&A, 47, 481 ADS
- Auer, L. H. & Mihalas, D. 1969a, ApJ, 156, 157 ADS
- Auer, L. H. & Mihalas, D. 1969b, ApJ, 156, 681 ADS
- Avrett, E. H. 1965, SAO Special Report, 174, 101 ADS
- Avrett, E. H. & Loeser, R. 1992, in Astronomical Society of the Pacific Conference Series, Vol. 26, Cool Stars, Stellar Systems, and the Sun, ed. M. S. Giampapa & J. A. Bookbinder, 489 ADS
- Avrett, E. H. & Loeser, R. 2008, ApJS, 175, 229 ADS
- Barklem, P. S., Piskunov, N., & O'Mara, B. J. 2000, VizieR Online Data Catalog, J/A+AS/142/467 ADS
- Baschek, B., Holweger, H., & Traving, G. 1966, Astronomische Abhandlungen der Hamburger Sternwarte, 8, 26 ADS
- Belluzzi, L., Trujillo Bueno, J., & Landi Degl'Innocenti, E. 2007, ApJ, 666, 588 ADS
- Bruls, J. H. M. J., Rutten, R. J., & Shchukina, N. G. 1992, A&A, 265, 237 ADS
- Cannon, C. J. 1973, ApJ, 185, 621 ADS
- Carlsson, M. 1986, Uppsala Astronomical Observatory Reports, 33 ADS
- Carlsson, M., Hansteen, V. H., Gudiksen, B. V., Leenaarts, J., & De Pontieu, B. 2016, A&A, 585, A4 ADS
- Carlsson, M. & Rutten, R. J. 1992, A&A, 259, L53 ADS
- Carlsson, M., Rutten, R. J., & Shchukina, N. G. 1992, A&A, 253, 567 ADS
- Carlsson, M. & Stein, R. F. 1994, in Chromospheric Dynamics, ed. M. Carlsson, 47 ADS
- Carlsson, M. & Stein, R. F. 1995, ApJL, 440, L29 ADS
- Carlsson, M. & Stein, R. F. 1997, ApJ, 481, 500 ADS
- Carlsson, M. & Stein, R. F. 2002, ApJ, 572, 626 ADS
- Cauzzi, G., Reardon, K., Rutten, R. J., Tritschler, A., & Uitenbroek, H. 2009, A&A, 503, 577 ADS
- Cram, L. E., Rutten, R. J., & Lites, B. W. 1980, ApJ, 241, 374 ADS
- da Silva Santos, J. M., de la Cruz Rodríguez, J., White, S. M., et al. 2020, A&A, 643, A41 ADS
- Danilovic, S. 2017, A&A, 601, A122 ADS
- del Toro Iniesta, J. C. 2007, Introduction to Spectropolarimetry ADS
- Del Zanna, G. & Mason, H. E. 2018, Living Reviews in Solar Physics, 15, 5 ADS
- Doyle, J. G., Jevremović, D., Short, C. I., et al. 2001, A&A, 369, L13 ADS
- Eddington, A. S. 1929, MNRAS, 89, 620 ADS
- Eklund, H., Wedemeyer, S., Snow, B., et al. 2021, Philosophical Transactions of the Royal Society of London Series A, 379, 20200185 ADS
- Ellerman, F. 1917, ApJ, 46, 298 ADS
- Falconer, D. A., Moore, R. L., Porter, J. G., & Hathaway, D. H. 1998, ApJ, 501, 386 ADS
- Feautrier, P. 1964, Comptes Rendus Academie des Sciences (serie non specifice), 258, 3189 ADS
- Fontenla, J. M., Avrett, E. H., & Loeser, R. 1993, ApJ, 406, 319 ADS
- Fontenla, J. M., Curdt, W., Haberleiter, M., Harder, J., & Tian, H. 2009, ApJ, 707, 482 ADS
- Fontenla, J. M., Stancil, P. C., & Landi, E. 2015, ApJ, 809, 157 ADS
- Fossum, A. & Carlsson, M. 2005a, Nat, 435, 919 ADS
- Fossum, A. & Carlsson, M. 2005b, ApJ, 625, 556 ADS
- Fossum, A. & Carlsson, M. 2006, ApJ, 646, 579 ADS
- Frogner, L., Gudiksen, B. V., & Bakke, H. 2020, A&A, 643, A27 ADS
- Golding, T. P., Leenaarts, J., & Carlsson, M. 2017, A&A, 597, A102 ADS
- Gray, D. F. 1977, ApJ, 218, 530 ADS
- Greve, A. & Zwaan, C. 1980, A&A, 90, 239 ADS
- Grottrian, W. 1931, Z. Astrophys., 3, 199 ADS
- Gudiksen, B. V., Carlsson, M., Hansteen, V. H., et al. 2011, A&A, 531, A154 ADS
- Heeck, J. 2013, Phys. Rev. Lett., 111, 021801 ADS

- Henriques, V. M. J., Kuridze, D., Mathioudakis, M., & Keenan, F. P. 2016, *ApJ*, 820, 124 [ADS](#)
- Hines, C. O. 1960, *Canadian Journal of Physics*, 38, 1441 [ADS](#)
- Holweger, H. 1967, *Z. Astrophys.*, 65, 365 [ADS](#)
- Holweger, H. & Müller, E. A. 1974, *SoPh*, 39, 19 [ADS](#)
- House, L. L. 1964, *ApJS*, 8, 307 [ADS](#)
- Houtgast, J. 1942, PhD thesis, - [ADS](#)
- Hubený, I. & Mihalas, D. 2014, *Theory of Stellar Atmospheres* (Princeton: Princeton University Press) [ADS](#)
- Jefferies, J. T. 1968, *Spectral line formation* (Waltham: Blaisdell) [ADS](#)
- Jefferies, J. T. & Thomas, R. N. 1959, *ApJ*, 129, 401 [ADS](#)
- Jordan, C. 1969, *MNRAS*, 142, 501 [ADS](#)
- Joshi, J., Rouppe van der Voort, L. H. M., & de la Cruz Rodríguez, J. 2020, *A&A*, 641, L5 [ADS](#)
- Keller, C. U. & von der Lühe, O. 1992, *A&A*, 261, 321 [ADS](#)
- Kostik, R., Khomenko, E., & Shchukina, N. 2009, *A&A*, 506, 1405 [ADS](#)
- Kostik, R. I. & Orlova, T. V. 1975, *SoPh*, 45, 119 [ADS](#)
- Kostik, R. I., Shchukina, N. G., & Rutten, R. J. 1996, *A&A*, 305, 325 [ADS](#)
- Kourganoff, V. 1952, *Basic methods in transfer problems; radiative equilibrium and neutron diffusion* (Oxford: Clarendon Press) [ADS](#)
- Krijger, J. M., Rutten, R. J., Lites, B. W., et al. 2001, *A&A*, 379, 1052 [ADS](#)
- Kurucz, R. L. 2009, in *Am. Inst. Phys. Conf. Series*, ed. I. Hubený, J. M. Stone, K. MacGregor, & K. Werner, Vol. 1171, 43–51 [ADS](#)
- LABS, D. & Neckel, H. 1972, *SoPh*, 22, 64 [ADS](#)
- Lambert, J., Paletou, F., Josselin, E., & Glorian, J.-M. 2016, *European Journal of Physics*, 37, 015603 [ADS](#)
- Landi Degl'Innocenti, E. & Landolfi, M. 2004, *Polarization in Spectral Lines*, Vol. 307 [ADS](#)
- Leenaarts, J. 2020, *Living Reviews in Solar Physics*, 17, 3 [ADS](#)
- Leenaarts, J. & Carlsson, M. 2009, in *Astronomical Society of the Pacific Conference Series*, Vol. 415, *The Second Hinode Science Meeting: Beyond Discovery-Toward Understanding*, ed. B. Lites, M. Cheung, T. Magara, J. Mariska, & K. Reeves, 87 [ADS](#)
- Leenaarts, J., Carlsson, M., Hansteen, V., & Rutten, R. J. 2007, *A&A*, 473, 625 [ADS](#)
- Leenaarts, J., Carlsson, M., & Rouppe van der Voort, L. 2012a, *ApJ*, 749, 136 [ADS](#)
- Leenaarts, J., Pereira, T., & Uitenbroek, H. 2012b, *A&A*, 543, A109 [ADS](#)
- Lemke, M. & Holweger, H. 1987, *A&A*, 173, 375 [ADS](#)
- Lin, Y., Engvold, O., & Rouppe van der Voort, L. H. M. 2012, *ApJ*, 747, 129 [ADS](#)
- Lites, B. W., Rutten, R. J., & Kalkofen, W. 1993, *ApJ*, 414, 345 [ADS](#)
- Livingston, W., Wallace, L., White, O. R., & Giampapa, M. S. 2007, *ApJ*, 657, 1137 [ADS](#)
- Lockyer, J. N. 1868, *Proceedings of the Royal Society of London Series I*, 17, 131 [ADS](#)
- Madjarska, M. S. 2019, *Liv. Rev. Solar Phys.*, 16, 2 [ADS](#)
- Madjarska, M. S., Chae, J., Moreno-Insertis, F., et al. 2021, *A&A*, 646, A107 [ADS](#)
- Malanushenko, O., Jones, H. P., & Livingston, W. 2004, in *Multi-Wavelength Investigations of Solar Activity*, ed. A. V. Stepanov, E. E. Benevolenskaya, & A. G. Kosovichev, Vol. 223, 645–646 [ADS](#)
- Maltby, P., Avrett, E. H., Carlsson, M., et al. 1986, *ApJ*, 306, 284 [ADS](#)
- Mihalas, D. 1970, *Stellar atmospheres* (San Francisco: W. H. Freeman and Co) [ADS](#)
- Mihalas, D. 1978, *Stellar atmospheres*, 2nd edition (San Francisco: W. H. Freeman and Co) [ADS](#)
- Minnaert, M. 1930, *Z. Astrophys.*, 1, 209 [ADS](#)
- Molnar, M. E., Reardon, K. P., Chai, Y., et al. 2019, *ApJ*, 881, 99 [ADS](#)
- Ng, K. C. 1974, *J. Chem. Phys.*, 61, 2680 [ADS](#)
- Nordlund, Å., Stein, R. F., & Asplund, M. 2009, *Living Reviews in Solar Physics*, 6, 2 [ADS](#)
- Olson, G. L., Auer, L. H., & Buchler, J. R. 1986, *J. Quant. Spectr. Rad. Transf.*, 35, 431 [ADS](#)
- Paletou, F. 2018, *Open Astronomy*, 27, 76 [ADS](#)
- Pereira, T. M. D. 2019, *Advances in Space Research*, 63, 1434 [ADS](#)
- Pereira, T. M. D., De Pontieu, B., Carlsson, M., et al. 2014, *ApJL*, 792, L15 [ADS](#)
- Pereira, T. M. D. & Uitenbroek, H. 2015, *A&A*, 574, A3 [ADS](#)
- Pottasch, S. R. 1964, *Space Sci. Rev.*, 3, 816 [ADS](#)
- Rouppe van der Voort, L., Leenaarts, J., de Pontieu, B., Carlsson, M., & Vissers, G. 2009, *ApJ*, 705, 272 [ADS](#)
- Rouppe van der Voort, L. H. M., De Pontieu, B., Hansteen, V. H., Carlsson, M., & van Noort, M. 2007, *ApJL*, 660, L169 [ADS](#)
- Rouppe van der Voort, L. H. M., Rutten, R. J., & Vissers, G. J. M. 2016, *A&A*, 592, A100 [ADS](#)
- Rutten, R. J. 1978, *SoPh*, 56, 237 [ADS](#)
- Rutten, R. J. 1988, in *Astrophys. Space Sci. Library*, Vol. 138, *IAU Colloq. 94: Physics of Formation of Fe II Lines Outside LTE*, ed. R. Viotti, A. Vittone, & M. Friedjung, 185–210 [ADS](#)
- Rutten, R. J. 1990, in *IAU Symposium*, Vol. 138, *Solar Photosphere: Structure, Convection, and Magnetic Fields*, ed. J. O. Stenflo, 501–516 [ADS](#)
- Rutten, R. J. 1995, in *ESA Special Pub.*, Vol. 376, *Helioseismology*, ed. J. T. Hoeksema, V. Domingo, B. Fleck, & B. Battrick, 151–163 [ADS](#)
- Rutten, R. J. 1999, in *Astron. Soc. Pacific Conf. Series*, Vol. 184, *Magnetic Fields and Oscillations*, ed. B. Schmieder, A. Hofmann, & J. Staude, Third Adv. in Solar Physics Euroconf., 181–200 [ADS](#)
- Rutten, R. J. 2002, *J. Astron. Data*, 8, 1 [ADS](#)
- Rutten, R. J. 2011, in *Indonesia Astronomy & Astrophysics*, ed. P. W. Premadi & et al. (Institut Teknologi Bandung: Indonesian Astron. Soc.), 3–8
- Rutten, R. J. 2016, *A&A*, 590, A124 [ADS](#)
- Rutten, R. J. 2017a, in *IAU Symposium*, Vol. 327, *Fine structure and dynamics of the solar atmosphere*, ed. S. Vargas Domínguez, A. G. Kosovichev, P. Antolin, & L. Harra, 1–15 [ADS](#)
- Rutten, R. J. 2017b, *A&A*, 598, A89 [ADS](#)
- Rutten, R. J. 2019, *SoPh*, 294, 165 [ADS](#)
- Rutten, R. J. 2020, *arXiv e-prints*, arXiv:2009.00376 [ADS](#)
- Rutten, R. J. & Carlsson, M. 1994, in *IAU Symposium*, Vol. 154, *Infrared Solar Physics*, ed. D. M. Rabin, J. T. Jefferies, & C. Lindsey, 309–322 [ADS](#)
- Rutten, R. J. & Kostik, R. I. 1982, *A&A*, 115, 104 [ADS](#)
- Rutten, R. J. & Krijger, J. M. 2003, *A&A*, 407, 735 [ADS](#)
- Rutten, R. J. & Milkey, R. W. 1979, *ApJ*, 231, 277 [ADS](#)
- Rutten, R. J., Rouppe van der Voort, L. H. M., & De Pontieu, B. 2019, *A&A*, 632, A96 [ADS](#)
- Rutten, R. J., Rouppe van der Voort, L. H. M., & Vissers, G. J. M. 2015, *ApJ*, 808, 133 [ADS](#)
- Rutten, R. J. & Uitenbroek, H. 1991, *SoPh*, 134, 15 [ADS](#)
- Rutten, R. J. & Uitenbroek, H. 2012, *A&A*, 540, A86 [ADS](#)
- Rutten, R. J., van Veelen, B., & Sütterlin, P. 2008, *SoPh*, 251, 533 [ADS](#)
- Rutten, R. J., Vissers, G. J. M., Rouppe van der Voort, L. H. M., Sütterlin, P., & Vitas, N. 2013, in *J. Physics Conf. Series*, Vol. 440, *Eclipse on the Coral Sea: Cycle 24 Ascending*, ed. P. S. Cally, R. Erdélyi, & A. A. Norton, 1–13 [ADS](#)
- Rutten, R. J. & Zwaan, C. 1983, *A&A*, 117, 21 [ADS](#)
- Rybicki, G. B. & Hummer, D. G. 1992, *A&A*, 262, 209 [ADS](#)
- Rybicki, G. B. & Lightman, A. P. 1986, *Radiative Processes in Astrophysics* (New York: Wiley), 400 [ADS](#)
- Scharmer, G. B. & Carlsson, M. 1985, *Journal of Computational Physics*, 59, 56 [ADS](#)
- Scharmer, G. B., Löfdahl, M. G., Slieden, G., & de la Cruz Rodríguez, J. 2019, *A&A*, 626, A55 [ADS](#)
- Sekse, D. H., Rouppe van der Voort, L., & De Pontieu, B. 2012, *ApJ*, 752, 108 [ADS](#)
- Sekse, D. H., Rouppe van der Voort, L., De Pontieu, B., & Scullion, E. 2013, *ApJ*, 769, 44 [ADS](#)
- Shchukina, N. G., Olshevsky, V. L., & Khomenko, E. V. 2009, *A&A*, 506, 1393 [ADS](#)
- Sheminova, V. A., Rutten, R. J., & Rouppe van der Voort, L. H. M. 2005, *A&A*, 437, 1069 [ADS](#)
- Smitha, H. N., Holzreuter, R., van Noort, M., & Solanki, S. K. 2020, *A&A*, 633, A157 [ADS](#)
- Smitha, H. N., Holzreuter, R., van Noort, M., & Solanki, S. K. 2021, *arXiv e-prints*, arXiv:2101.00506 [ADS](#)
- Straus, T., Fleck, B., Jefferies, S. M., et al. 2008, *ApJL*, 681, L125 [ADS](#)
- Sukhorukov, A. V. & Leenaarts, J. 2017, *A&A*, 597, A46 [ADS](#)
- Sütterlin, P., Rutten, R. J., & Skomorovsky, V. I. 2001, *A&A*, 378, 251 [ADS](#)
- Thomas, R. N. 1957, *ApJ*, 125, 260 [ADS](#)
- Uitenbroek, H. 2000, *ApJ*, 531, 571 [ADS](#)
- Uitenbroek, H. 2001, *ApJ*, 557, 389 [ADS](#)
- Uitenbroek, H. & Bruls, J. H. M. J. 1992, *A&A*, 265, 268 [ADS](#)
- Uitenbroek, H. & Criscuolo, S. 2011, *ApJ*, 736, 69 [ADS](#)
- Unruh, Y. C., Solanki, S. K., & Fligge, M. 1999, *A&A*, 345, 635 [ADS](#)
- Unsöld, A. 1955, *Physik der Sternatmosphären* (2. Auflage, Springer) [ADS](#)
- van Noort, M., Rouppe van der Voort, L., & Löfdahl, M. G. 2005, *SoPh*, 228, 191 [ADS](#)
- Vernazza, J. E., Avrett, E. H., & Loeser, R. 1976, *ApJS*, 30, 1 [ADS](#)
- Vernazza, J. E., Avrett, E. H., & Loeser, R. 1981, *ApJS*, 45, 635 [ADS](#)
- Vissers, G. J. M., Rouppe van der Voort, L. H. M., & Rutten, R. J. 2013, *ApJ*, 774, 32 [ADS](#)
- Vissers, G. J. M., Rouppe van der Voort, L. H. M., & Rutten, R. J. 2019, *A&A*, 626, A4 [ADS](#)
- Vissers, G. J. M., Rouppe van der Voort, L. H. M., Rutten, R. J., Carlsson, M., & De Pontieu, B. 2015, *ApJ*, 812, 11 [ADS](#)
- Vitas, N., Viticchiè, B., Rutten, R. J., & Vögler, A. 2009, *A&A*, 499, 301 [ADS](#)
- Vögler, A., Shelyag, S., Schüssler, M., et al. 2005, *A&A*, 429, 335 [ADS](#)
- Watanabe, H., Vissers, G., Kitai, R., Rouppe van der Voort, L., & Rutten, R. J. 2011, *ApJ*, 736, 71 [ADS](#)
- Whitaker, W. A. 1963, *ApJ*, 137, 914 [ADS](#)
- Wiersma, J., Rutten, R. J., & Lanz, T. 2003, in *Astron. Soc. Pacific Conf. Series*, Vol. 288, *Stellar Atmosphere Modeling*, ed. I. Hubený, D. Mihalas, & K. Werner, 130–136 [ADS](#)
- Wijbenga, J. W. & Zwaan, C. 1972, *SoPh*, 23, 265 [ADS](#)
- Withbroe, G. L. 1978, *ApJ*, 225, 641 [ADS](#)
- Zirin, H. & Popp, B. 1989, *ApJ*, 340, 571 [ADS](#)